Construction and Building Materials

REPAIR OF SEVERELY DAMAGED RC COLUMNS THROUGH FRCM COMPOSITES

--Manuscript Draft--

Manuscript Number:	CONBUILDMAT-D-20-08453R1
Article Type:	Research Paper
Keywords:	Composites; concrete damage; confinement; interaction; FRCM; repair; RC columns
Corresponding Author:	Flora Faleschini University of Padova Padova, ITALY
First Author:	Klajdi Toska
Order of Authors:	Klajdi Toska
	Flora Faleschini
	Mariano Angelo Zanini
	Lorenzo Hofer
	Carlo Pellegrino
Abstract:	This study presents the results of an experimental campaign aimed at testing the effectiveness of carbon fiber reinforced cementitious matrix (CFRCM) confinement as a repair technique for severely damaged reinforced concrete (RC) columns. To evaluate shape effect and transverse steel reinforcement (TSR) – fiber interaction, two different cross-section shapes, and two TSR rates were investigated. Nine full-scale specimens were analyzed considering three control ones, three undamaged specimens confined with two CFRCM layers, and three severely damaged specimens repaired through confinement by two CFRCM layers. Axial stress-strain curves were analyzed to derive strength and ductility enhancement. Finally, TSR and fiber strains were monitored to better comprehend the contributions of internal and external reinforcement to the overall confinement and possible TSR-FRCM interaction.

DIPARTIMENTO DI INGEGNERIA CIVILE, EDILE E AMBIENTALE - I C E A
DEPARTMENT OF CIVIL, ENVIRONMENTAL AND ARCHITECTURAL ENGINEERING

UNIVERSITÀ DEGLI STUDI DI PADOVA

Via F. Marzolo, 9 - I 35131 Padova
tel +39 049 8275424 fax +39 049 8275446

C.F 80006480281 - P.IVA 00742430283

November, 5th 2020

Dear Editor of the Journal Construction and Building Materials

please find enclosed the revised version of the manuscript:

"REPAIR OF SEVERELY DAMAGED RC COLUMNS THROUGH FRCM COMPOSITES"

By Klajdi Toska, Flora Faleschini, Mariano Angelo Zanini, Lorenzo Hofer and Carlo Pellegrino

for possible publication in the Journal Construction and Building Materials.

Sincerely,
Flora Faleschini

Flora Faleschini, Ph.D., Assist. Prof.
Department of Civil, Environmental and Architectural Engineering
University of Padova
via Marzolo, 9
35131 Padova - Italy
flora.faleschini@dicea.unipd.it

REPAIR OF SEVERELY DAMAGED RC COLUMNS THROUGH FRCM COMPOSITES

Klajdi Toska[1], Flora Faleschini[1,*], Mariano Angelo Zanini[1], Lorenzo Hofer[1] and Carlo Pellegrino[1]

[1] Department of Civil, Environmental and Architectural Engineering, University of Padova, via Francesco Marzolo 9, Padova, Italy.

[*] corresponding author: flora.faleschini@dicea.unipd.it

ABSTRACT

This study presents the results of an experimental campaign aimed at testing the effectiveness of carbon fiber reinforced cementitious matrix (CFRCM) confinement as a repair technique for severely damaged reinforced concrete (RC) columns. To evaluate shape effect and transverse steel reinforcement (TSR) – fiber interaction, two different cross-section shapes, and two TSR rates were investigated. Nine full-scale specimens were analyzed considering three control ones, three undamaged specimens confined with two CFRCM layers, and three severely damaged specimens repaired through confinement by two CFRCM layers. Axial stress-strain curves were analyzed to derive strength and ductility enhancement. Finally, TSR and fiber strains were monitored to better comprehend the contributions of internal and external reinforcement to the overall confinement and possible TSR-FRCM interaction.

Keywords: composites, concrete damage, confinement, interaction, FRCM, Repair, RC columns.

1. INTRODUCTION

Composites are now common materials in retrofitting existing under-designed reinforced concrete (RC) structures. The use of Fiber Reinforced systems has been on the focus of many studies since the early 70s even though a broad use of the technique started much later [1,2]. Until lately, composite materials used for rehabilitation of concrete or masonry structures were generally applied through organic matrix (epoxy-based), guaranteeing a significant improvement for both resistance and ductility properties of the strengthened element.

Confinement is one of the main techniques used to retrofit axially loaded elements. Fiber Reinforced polymer (FRP) systems permit to easily confine existing RC elements by wrapping continuously or partially FRP strips, enhancing their axial strength and ductility without a significant increase in weight or lateral stiffness [3-6]. Confinement by FRP systems has proven to be effective also for repairing RC elements damaged due to excessive axial loading or seismic events. Several research works have been carried out to investigate repair effectiveness of FRP confinement both on plain and reinforced concrete. Saadatmanesh et al. [7] investigated the effectiveness of repairing earthquake-damaged RC columns with FRP wraps. Four different specimens were tested under lateral cyclic loading to simulate the seismic effect on the elements, which were then repaired through FRP wraps and re-tested under the same protocol. In general, all repaired specimens performed well under the cyclic loading test, showing an increase in lateral strength varying from 1 to 38%. Li et al. [8] conducted an experimental campaign on 24 RC specimens tested under uniaxial compression that were formerly damaged through split tensile tests. On the other hand, Faleschini et al. [9] investigated experimentally the effectiveness of FRP composites to repair severely-damaged exterior RC beam-column joints, verifying also the contribution of the FRP system on the overall shear capacity of the joints through some analytical models. Some researchers have also experimentally investigated the effect of the combined FRP-steel confinement on the behavior of concrete columns. Eid & Paultre [10] presented a designed-oriented confinement model for assessing the axial and lateral behavior of circular concrete columns confined with steel ties, FRP composites, and both of them. Teng et al.

[11] proposed a stress-strain model for concrete under combined confinement from FRP and TSR, which has been derived in two alternative versions seeking for increasing accuracy of the prediction. Subsequently, Lin et al. [12] presented a design-oriented stress-strain model for concrete under the combined FRP-steel confinement for circular RC columns, showing a good balance between accuracy of the prevision and simplicity of form. Al-Rahmani & Rasheed [13] proposed a confinement model for combined external FRP – internal TSR confinement for rectangular RC columns. Lately, Kaeseberg et al. [14] conducted an extensive experimental research on 63 CFRP-confined plain concrete columns and 60 CFRP-TSR confined specimens, analyzing the influence on the confinement efficiency of different parameters. Finally, a modified stress-strain and ultimate condition design model was proposed.

However, the use of epoxy resins brings some important liabilities to FRP systems. Poor fire resistance [15], difficult application on wet surfaces, low breathability of the substrate, low reversibility [16], and high sensitivity to UV radiations [17] have led to a lower use of FRP systems in favor to new, more compatible and durable solutions. A similar but alternative solution was born from replacing the organic (epoxy) matrix with inorganic cement-based one, generally known as Fiber Reinforced Cementitious Mortar (FRCM) or Textile Reinforced Mortars (TRM). Like FRP systems, FRCMs have been broadly used lately to enhance flexural [18-21] and shear [22-25] strength of beam elements and to enhance axial strength and ductility of concrete or masonry columns through confinement [26-33].

Concrete confinement through FRCM systems has been the subject of many experimental campaigns and research activities. Tests are mainly based on small-scale non-reinforced elements. Triantafillou et al. [33] were one of the first to analyze the effectiveness of confinement through TRM with respect to the more consolidated FRP systems. Results proved that TRM jackets provided a significant increase in strength and ductility to plain concrete specimens, even though this solution resulted slightly less effective than the FRP counterpart. More recently, Colajanni et al. [29] analyzed the effect of fiber ratio, cross-section shape and corner radius in FRCM confined specimens tested under

monotonic and cyclic axial loading. Ombres et al. conducted several experimental campaigns [30-31] on small-scale plain concrete specimens confined with FRCM systems and later proposed a prediction model based on experimental data collected from different research works [32]. Gonzalez-Libreros et al. [34] also analyzed confinement of plain concrete specimens using CFRCM and GFRCM (the former with carbon, and the latter with glass fibers). The investigation included also the monitoring of hoop strains developed on fibers, to better understand the influence of fiber properties on the FRCM confinement effectiveness. The study showed that fiber exploitation ratio and final confinement effectiveness strongly depends on fabric properties used in the FRCM system. On the other hand, less experimental work can be found on FRCM confinement of real-scale reinforced concrete elements. Bournas et al. [35] investigated confinement effectiveness of FRCM on small-scale RC specimens tested under uniaxial compression loading and on nearly full-scale RC columns tested under cyclic lateral loading. Results showed that FRCM jacketing effectiveness was similar to that of specimens confined with FRPs even though a slight difference of nearly 10% was observed on the uniaxial compressive tests. Recently, some of the authors have investigated confinement effectiveness of FRCM systems on full-scale RC columns comparing different cross-section shapes and steel reinforcement configurations using carbon fibers [36] and glass fibers [37]. Both studies investigated strain development both on transverse steel reinforcement and on confining fibers to evaluate the influence of the axial rigidity of the composites on the effectiveness of the FRCM system and the interaction between internal transverse steel reinforcement and the external FRCM confinement.

While FRCM systems have proven to confer an adequate level of confinement to existing concrete elements, little work has been done to evaluate their effectiveness in the repair of damaged RC elements by excessive axial loads or, as often happens, by seismic loads. Few studies have been carried out on small-scale plain concrete specimens, worth mentioning Peled [38] who studied confinement of damaged and undamaged concrete elements with FRP and FRCM systems. Results showed that composite systems were able to provide an adequate enhancement of axial strength and

ductility even for specimens with initial damage conditions. The effectiveness was observed also by Gonzalez-Libreros et al. [39], where small-scale plain concrete specimens were initially damaged through post-peak compressive loading, then confined by CFRCM and re-tested under monotonic axial load. Results showed that CFRCM confinement was able to restore the original axial capacity of the specimens.

However, on the best authors' knowledge, the few experimental works cited above on the effectiveness of FRCM jackets on damaged axially-loaded columns dealt only with small scale specimens, and considered only plain concrete (without any internal reinforcement). The present paper's goal is to investigate the effectiveness of CFRCM composites to adequately repair severely damaged RC columns. The experimental campaign considers different cross-section shapes (circular and squared), different internal reinforcement configurations and compares the results of unconfined RC members, CFRM confined specimens with undamaged conditions (strengthened) and CFRCM confined specimens with severe damage conditions (severely-damaged and repaired). In addition, hoop strains of transverse steel reinforcement (TSR) and external fiber reinforcement have been investigated to better understand fiber exploitation and steel-fiber interaction in specimens with different initial conditions.

2. MATERIALS AND EXPERIMENTAL PROGRAM

2.1 Test specimens

The research program deals with the study of nine RC samples, which differ by the following variables: cross-section shape; inner transverse reinforcement amount; concrete damage presence or not; presence of FRCM jacket or not. Specimens' main features are described in Table 1. Overall, it is possible to classify them in three main categories: unconfined; strengthened; severely-damaged and repaired.

All the columns present the same height h = 1000 mm and concrete cover c = 20 mm. Two cross-section geometries are investigated, a circular one *C* with diameter d = 300 mm; and a squared one *S*

with size l = 300 mm. In this latter case, the same corner radius r of 20 mm was used in all the prismatic columns. Concerning the inner reinforcement, details are shown in Figure 1: there, it is possible to observe how for all the test specimens the same longitudinal steel reinforcement (A_{sl}) is adopted, consisting in four 14-mm diameter bars, equally spaced in the cylinders and placed at section edges in the prisms. Conversely, the amount of TSR (A_{sw}) varies adopting two configurations. Cylinders present only one single TSR type, consisting in circular hoops with 8-mm diameter bars, placed each 200 mm in the central part of the specimen. Two legged stirrups with 8-mm diameter bars are used instead in prismatic specimens, adopting two spacings in central region of the columns, namely 200 and 330 mm. Steel reinforcement bar properties were the same for all the configurations, and they were experimentally evaluated on three specimens per each type through tensile tests, being f_y = 552 ± 10 MPa at ε_y = 0.002, f_t = 650 ± 15 MPa at ε_t = 0.090 for the longitudinal 14-mm diameter bars, and f_y = 485 ± 15MPa at ε_y = 0.002, f_t = 630 ± 18 MPa at ε_t = 0.090 for the transverse 8-mm diameter bars, respectively.

To realize the specimens, two different concrete batches were used due to laboratory constraints, aiming in both cases at attaining a cylinder compressive strength class at 28 days of about C16/20 according to [40], that however present some differences in terms of strength and elastic properties in the two mixes. Indeed, the following experimental results (evaluated on three specimens per type and per each analyzed feature, i.e., compressive strength, tensile strength and secant elastic modulus, at 28 days) were obtained: f_{c1} = 24.1 ± 0.74 MPa, f_{ct1} = 1.15 ± 0.26 MPa, E_{c1} = 33.3 ± 4.25 GPa for the first batch; f_{c2} = 17.4 ± 2.04 MPa, f_{ct2}= 1.10 ± 0.14 MPa, E_{c2} = 19.2 ± 0.95 GPa for the second one. It is worth to recall that each trio of unconfined, confined and damaged-repaired specimens is realized with the same mix, for sake of comparison purposes. Further, three columns are labelled as damaged ones, this meaning that damaged specimens are the same unconfined columns (named as NC*)* subject to the loading protocol (described in Section 2.3) and then repaired. Hence, a direct comparison between the performance of unconfined and damaged-repaired specimens is possible.

Lastly, the specimens could be unconfined or confined, and in this latter case the FRCM jacket is realized through two-fiber layers of carbon-FRCM composite, which characteristics are reported in Section 2.2. The two-layers confinement choice was made based on a previous experimental campaign carried out by some of the authors on damaged plain concrete cylinders confined with the same fiber type obtaining strength enhancement between 10 and 20% when using this confinement configuration [39]. Overall, six samples over nine were confined.

2.2 Externally-bonded composite properties

The FRCM system was realized using balanced bidirectional carbon fiber sheets and a single-component mortar (CFRCM system). The fibers' characteristics declared by the producer were integrated by some experimental tests, needed to experimentally assess the tensile strength (f_u) and elastic modulus (E_f) values. To sum up, the properties of the carbon fiber, resulted from tests on three specimens, are: overall area weight W = 170 g/m^2, fiber elastic modulus E_f = 242 GPa, fiber tensile strength f_u = 1487 (MPa) at ultimate tensile strain ε_{fu} = 1.1%, equivalent nominal thickness t_f = 0.047 mm. The mortar is a fiber-reinforced pre-mixed one, hydrated at a water/binder ratio ranging between 0.18 and 0.22. For the repair operation, the same mortar was used. Mechanical properties (compressive and flexural strength) were experimentally evaluated according to EN 1015-11 [41], on 40x40x160 mm prisms that were casted during the repair and strengthening operations, and tested the same day of RC columns, and they are reported in Table 2 per each realized column. Values refer to average results measured at least on three samples per each analyzed property.

2.3 Experimental protocol: loading, test setup, repair and retrofit operations

The same experimental loading protocol was used for all the tested specimens, and it involves an axial loading of the columns through a displacement-control mode, during which concrete axial strains ($\varepsilon_{c,yy}$), strains into both TSR ($\varepsilon_{s,xx}$) and CFRCM fibers ($\varepsilon_{f,xx}$) were simultaneously acquired. The load was applied at a rate of 0.3mm/min, similarly than in [37], directly onto the top of the RC column, using a a 10MN capacity testing machine which mounted a 6MN capacity load cell for the continuous acquisition of the signal. In the unconfined specimens, the load was stopped after a pre-imposed

damage condition of about 30%, identified as the point in the post-peak branch corresponding to the 0.70 of the peak load (P_{max}), was reached. Such damage level is considered very significant, also compared to other works in literature aimed at verifying the effectiveness of repair systems to damaged RC specimens, where typically such value is set around 20% but might arise up to 50% [42,43].

Concerning the instrumentation used to acquire concrete axial strains, they were monitored using two types of devices, the former to describe the pre-peak and the latter to better capture the post-peak branch. In the previous case, three mechanical strain gages (mSGs), with a gauge length of 250 mm, were mounted onto the columns (cylinder) external surface at mid-height, equally spaced at 120°. In case of prismatic samples, four mSGs were used, with the same characteristics, but placed onto each sample face. Further, two linear voltage displacement transducers (LVDTs) were adopted to measure the movement of the plate mounted at each column top. Transverse strains were monitored both in the steel and in the CFRCM composite through the application of electric strain gages (eSGs). Particularly, four were applied onto the central stirrup at the column mid-height before casting operations, to evaluate TSR strains ($\varepsilon_{s,xx}$). Four were also used to evaluate fiber strains ($\varepsilon_{f,xx}$), applying directly the strain gages onto the carbon sheet, being two per each layer and located in the same position in opposite faces. Their disposition, depending on the specimen type, is shown in Figure 2. It is worth to recall that all the measures were recorded with same acquisition unit, at same frequency fixed at 5Hz.

For the damaged specimens, before the application of the FRCM jacket, a repair protocol was followed. First, an inspection of damaged regions of the tested unconfined specimens was carried out, removing the loose concrete with a hammer, and cleaning the surface with an air compressor. The appearance of the specimens at this stage is shown in Figure 3a. Then, the section of the columns was restored to the original size, using the mortar type described in Section 2.2, applying it in layer of maximum 30 mm per time as recommended by the producer, and whose characteristics are listed in Table 2. Before placing the mortar into the formwork, the concrete of the original specimens was

wetted to enhance the bond between the two materials. Lastly, after repair operation (see Figure 3b), concrete surface was superficially damped and covered with plastic wrap for one week.

Concerning instead CFRCM jacketing operation, this was carried out after 28 days from specimens manufacturing in case of strengthened ones, and after 28 days from the repair operation in case of severely-damaged samples. In both cases, the application of the composites followed the same procedure: first, specimens' surface was wetted to homogenously hydrate the support; then, a first layer of mortar was applied (Figure 4a), with an average thickness of 3 mm; the first layer of carbon sheet (instrumented with the eSGs) was then allowed to adhere to the mortar, gentle pushing into the matrix; then, the same procedure was repeated, ensuring the sheet to have an overlapping length of about 200 mm. The choice of the overlapping length used was based on a literature review on bond between FRCM systems and concrete substrates. Ombres [44] and D'Ambrisi [45] investigated bond behavior in PBO FRCM – Concrete systems reporting an effective bond length ranging between 150 mm and 200 mm; Caggegi et al. [46] reported an effective bond length related to Basalt TRM strengthening system of approximately 125 mm; Raof et al. [47] found that the effective bond length is in the range of 200-300 mm depending on the examined number of layers used. The overall thickness of the two CFRCM layers jacket was about 8 mm. It is worth to recall that the sheet was cut having an overall height of about 980 mm, thus leaving about 10 mm of empty surface per side, at the top and bottom of the specimen (Figure 4b).

3. RESULTS

3.1 Cracking pattern

All nine specimens were tested under monotonical axial compressive load while carefully monitoring axial stresses and strains, crack propagations, and strains development in the inner transverse steel reinforcement and in the outer fiber reinforcement. Collapse achievement, for the sake of comparison, is herein conventionally defined as a 20% reduction of the maximum attained load, both for confined and unconfined specimens, even though loading has been stopped at about 30% of the maximum load

drop in the unconfined specimens. Cracks opening and propagation were monitored during the loading history.

For the unconfined specimens, relevant visible cracking patterns occurred mainly in the post-peak branch, while for the confined specimens cracking displayed much earlier. For these latter, all cylinder specimens displayed a quite uniform cracking pattern in the pre-peak loading while in the post-peak loading very few new openings were observed (Figure 5). Instead, for the squared columns, existing cracks at the overlapping zone and near the edges grew at a higher rate in the post-peak branch than in the pre-peak one. Severely-damaged specimens displayed similar cracking patterns to the undamaged jacketed ones, even though more homogeneous vertical cracks were observed in the damaged squared columns compared to the undamaged ones. It is worth highlighting that confined specimens with higher TSR spacing displayed a wider cracking pattern in both damaged and undamaged conditions.

3.2 Axial stress-strain behavior

3.2.1 Undamaged bare vs. strengthened specimens

The analyzed columns were cast in two different moments resulting in two different concrete batches, having different compressive strengths but also elastic moduli as highlighted in section 2. For both batches, important enhancements of the properties were observed even though some differences in the overall axial behavior, that will be shown hereafter, may be due to such initial concrete difference. Axial behavior is discussed principally in terms of peak axial strength (f_{c0}) and corresponding axial strain (ε_{c0}), ultimate concrete stress (f_{cu}) (at 0.8 P_{max}) and corresponding ultimate axial strain (ε_{cu}) for the results of the unconfined specimens. For the confined specimens, results are presented in terms of confined axial strength (f_{cc}) and corresponding axial strain (ε_{cc}), confined ultimate stress (f_{ccu}) and corresponding ultimate axial strain (ε_{ccu}). Concrete axial stresses are computed deducing from the load recorded by the load cell the amount beared by the longitudinal bars, and then dividing it by the section area of the concrete. Recall that failure condition is conventionally considered at $0.8P_{max}$ but since the load beared by the longitudinal bars is deduced when computing concrete axial stresses, f_{cu}

(or f_{ccu}) does not correspond to 0.8 f_{c0} (or f_{cc}). Axial stress-strain curves are shown in Figure 6 comparing each trio of unconfined (continuous line), strengthened (dashed), and severely-damaged repaired (dotted) specimens.

Clear enhancements of peak strength and peak strain are observed for C20 and S33 confined specimens compared to the unconfined counterparts. Instead, an inconsistent behavior was observed for the S20_D0_C2 specimen: improvements were observed only in terms of ultimate strain, while axial strength remained almost invariant with respect to the unconfined S20_NC counterpart. Even though the same concrete batch was used for both these specimens, differences in concrete compaction and curing is believed to be the cause of this lack of improvement. Also quite low fiber strains were recorded at concrete peak strain for this specimen compared to the S33_D0_C2 and C20_D0_C2 ones. The main parameters resulting from the tests are listed in Table 3.

For undamaged specimens the best results, as expected, are obtained for the circular cross-section column with 34% increase in peak axial strength (f_{cc}) and 28% in peak strain (ε_{cc}). The squared section column S33, which also had a higher TSR spacing, showed a 27% improvement in axial strength and only 10% in peak strain. For the S20 specimen, for the reasons mentioned above, strength enhancement was limited but an important increase of 22% was observed in peak strain and nearly 30% in ultimate strain. On the other hand, S33_D0_C2 column was the only to record a slightly lower ultimate strain (92.5%) with respect to the unconfined specimen.

3.2.2 Severely-damaged repaired specimens

The main focus of the presented experimental work is to assess the effectiveness of CFRCM confinement on repairing severely-damaged RC columns, and quite promising results were observed for the three specimen types considered, as shown in Figure 6. A clear improvement in terms of axial strength with respect to the damaged conditions is observed for all specimens. As for the undamaged columns, the best performance was observed for the C20 geometry which was able to equal the attained load of the undamaged strengthened specimen, showing an increase of nearly 34% in axial strength with respect to the unconfined case. In the square-section columns, as expected, CFRCM

confinement resulted less effective than their analogue circular one. The repair was able to restore the initial strength of S20_NC (with also 3% gain) in the S20_D1_C2 specimen; instead, in the S33_D1_C2 the repair procedure was able to restore only 90% of the initial unconfined strength of S33_NC (see Table 3).

Looking at the overall stress-strain curves of undamaged specimens, in the pre-peak branch no significant differences in the axial stiffness are noted between unconfined and confined columns. As can be seen in Figure 6, differences are observed only after stress values near to f_{c0} value. On the other hand, damaged specimens show immediately a reduced axial stiffness due to their damaged condition. But while specimens with the same TSR spacing (s = 200 mm) show similar elastic modulus reduction regardless of the cross-section shape, specimen S33_D1_C2 displays a more pronounced difference between undamaged and damaged secant modulus since relatively small stress values (nearly to 6 MPa). As damage level is relatively similar in all specimens, it is believed that TSR high spacing is the main factor to which this difference is due.

When considering undamaged RC columns confined with CFRCM, the confinement system effectiveness seems similar in terms of peak strength (f_{c0}) and strain (ε_{cc}) development, with gains varying in the order of 10-34%, as discussed in section 3.2.1. This is not the case when dealing with severely damaged columns. The CFRCM system for the damaged columns with the lowest TSR spacing (i.e., C20 and S20) was able to restore at least the initial strength of the unconfined specimens. However, in none of the above, it was possible to restore the peak strain of the unconfined specimens, reaching only 65% and 78% of ε_{c0}, respectively. The confined damaged specimen with the highest TSR spacing (i.e., S33_D1_C2) could not restore the initial unconfined strength, probably due to its lower axial stiffness previously discussed, and reached its peak strength at an axial strain 10% higher than its unconfined case.

However, when assessing the effectiveness of CFRCM confinement on repairing severely-damaged RC elements, the authors believe that it is not entirely appropriate to refer to the initial resistance of the undamaged condition only. Indeed, since repairing is done on an already damaged element, it

results more significant to evaluate the effectiveness of the intervention referring to the residual axial strength of the columns at the end of the previous loading history. In Table 3, the residual axial strength values for each unconfined specimens are reported under the parameter $f_{u,D,}$ and the effectiveness of the repair operation is evaluated through the $f_{cc}/f_{u,D}$ ratio. It can be seen that through the CFRCM confinement, all repaired specimens have significantly enhanced their residual axial capacity. The circular-shaped section is still the most effective with an increment of the repaired axial capacity with respect to the residual capacity of the severely-damaged element of nearly 118%. The squared-shape sections result less effective than the circular one, but were still able to enhance their damaged residual capacity by 73% for the S20_D1_C2 and by 41% for the S33_D1_C2 specimen. It is important to highlight how, apart from the influence of the cross-section shape in the effectiveness of the CFRCM confinement, the spacing of internal TSR is of fundamental importance in the overall confinement effectiveness.

3.2 Fiber and TSR strain development

Strain development was monitored in all specimens in the central stirrup using four eSGs and in the FRCM layers for the externally confined specimens using two eSGs per layer applied on the opposite faces of the columns, as better detailed in Section 2.3. Results are shown in Figures 7-8 for unconfined (continuous line), strengthened (dashed), and severely-damaged repaired (dotted) specimens. Fully opaque lines represent the mean strain values while transparent lines show the trend of single eSGs.

3.2.1 TSR strains

Figure 7 shows in detail TSR strains evolution in (a) C20, (b) S20 and (c) S33 columns, in all the three analyzed conditions. The circular-section C20 geometry recorded the lowest strains compared to the square-section columns for all three considered conditions. Particularly low strain values were recorded in the unconfined and strengthened specimens (i.e., C20_NC and C20_D0_C2). This may be due to damage concentration on the upper part of the column which may have solicited more those stirrups in the highest positions (see Figure 5), which unfortunately were not being monitored.

For the undamaged columns, strains in the TSR grow at the same rate in both confined and unconfined elements. A slight difference is noted only in the S33 undamaged specimens, where at axial stress of about 9 MPa the TSR strain rate becomes slightly higher for the unconfined specimen. Generally, TSR strains development started earlier for damaged specimens, which also developed higher values than the undamaged ones. It is interesting to notice the difference in the strain rate development between circular- and square-section columns. Strain rates in the pre-peak branch of the curve result much higher for the squared shape sections, while the circular one shows strain rates closer to the undamaged conditions, which grow faster at axial stress levels near to the unconfined strength (f_{c0}). For damaged square-section columns (i.e., S20_D1_C2 and S33_D1_C2) TSR strains grow at higher rates after stress levels of about 0.25-0.30 f_{cc}.

Table 4 reports mean strain values for TSR and FRCM at peak and ultimate stresses. Comparing TSR strains at peak load among undamaged specimens, very similar values are recorded. $\varepsilon_{s,xx}$ of the C20_NC is a little less than 0.1‰, while also the confined one C20_D0_C2 recorded strains slightly above 0.1‰. The squared S20 undamaged specimens recorded also similar TSR strains of nearly 0.18‰ and 0.20‰, respectively for the unconfined and confined situations. On the other hand, the S33 specimens recorded lower TSR strains in the confined condition (0.33‰) with respect to the unconfined one (0.68‰). It seems that higher TSR strain values at peak stress are recorded in specimens with less effective confinement systems, both in terms of section-shape and reinforcement spacing. This order is maintained also for TSR strains at ultimate stress with higher strains recorded in the S33 column followed by the S20 and C20 ones.

Discussing the strain evolutions on damaged columns (i.e., those specimens labelled with “D1”), the results show TSR strains at peak load that are almost five times higher than the ones recorded in the confined but undamaged cases (i.e., D0). C20_D1_C2 specimen recorded a mean TSR strain of 0.5‰ (instead of 0.1‰ recorded in C20_D0_C2), S20_D1_C2 TSR strain was about 1.1‰ (instead of 0.2‰ in S20_D0_C2) and the same trend was observed in the S33 geometry, where the damaged case S33_D1_C2 recorded 1.58‰ (instead of 0.33‰ in S33_D0_C2).

3.2.2 Fiber and TSR strains in the confined columns

Measuring local strains in the FRCM jacketing experimentally is a harsh task and not always repays with the expected results. The possibility that cracks open at eSG location or that eSGs are located between two cracks, being so affected by tension stiffening phenomena, may result in quite variable strain records. To guarantee reliable results, high numbers of eSGs distributed through the reinforcement layers must be applied, but this cost efforts and especially can result uneconomic. However, in this experimental campaign good results were obtained also for the monitored fiber strains. Few eSGs with discordant records were discarded from the final results. Figure 8 compares TSR and fiber strains in the damaged specimens in (a) C20_D1_C2, (b) S20_D1_C2 and (c) S33_D1_C2 specimens, while fiber strain values at peak and ultimate stress are listed in Table 5, in its last two columns. In the pre-peak condition, C20_D1_C2 and S33_D1_C2 develop TSR and fiber strains at almost the same rate. In the S20_D1_C2 specimen, significant fiber strains were recorded only after stress levels of nearly 0.6 f_{cc}, while TSR strains start growing almost immediately. Different trends are observed in the post-peak branch for circular- and square-section specimens. In the C20_D1_C2 specimen, after peak stress, fiber strains grow at higher rate than TSR strains. This means that the FRCM system plays a bigger role than the TSR in the axial ductility of the confined RC element. In both square-section columns, TSR and fiber strains follow almost the same trend in the post-peak behavior, with TSR final strains being slightly higher than the fiber ones in the S20 case and almost the same strains in the S33 geometries. Peak strains recorded in TSR and fibers were quite similar in all specimens, with some differences only in the S33 specimen. The circular-section column C20_D1_C2 recorded lower peak strain values (0.4‰ for fibers and 0.5‰ for TSR) compared to those in squared columns, which were more than the double. On the other hand, fiber strains at ultimate stress were higher in the circular shaped section, which explains, along with the more effective section shape, the slightly more ductile behavior this specimen showed (Figure 6).

It is also worth mentioning that in C20 and S20 specimens no significant differences were noted in the strains recorded in the different layers of the CFRCM system while in the S33 specimens fiber exploitation resulted higher in the first CFRCM layer.

4. DISCUSSION

4.1 Cross-section geometry effect

Cross-section shape is known to be an important factor when dealing with confinement systems and its influence remains important even when repairing damaged RC elements. Figure 9 compares axial stress-strain curves relative to the initial strength of unconfined specimens f_{c0} (a) and to the remaining capacity of the damaged specimens $f_{u,D}$ (b). Cross-section shape effect is evident when comparing C20 and S20 geometries, characterized by the same TSR and fiber rate. C20_D1_C2 specimen results nearly 30% more effective than the squared-shape column in terms of both $f_{cc}/f_{u,D}$ and f_{cc}/f_{c0} rates. On the other hand, TSR influence on the overall behavior of the repaired elements is well highlighted comparing specimens S20 and S33, that differ only by the stirrups spacing (i.e. 200 and 330 mm). The effect of stirrup spacing is clearer in Figure 9.b, which considers the repaired strength f_{cc} with respect to the residual strength $f_{u,D}$ of the damaged specimens. The repaired S20 specimen resulted 25% more effective than the same specimen with 330 mm stirrup spacing (S33). Comparing f_{cc}/f_{c0} rates only, the S20 specimens would result only 14% more effective than the S33. These results indicate that cross-section shape and fiber-TSR interaction can significantly influence the overall behavior of damaged elements repaired through CFRCM confinement.

Cross-sectional shape influences also the development of lateral strains in TSR and fiber reinforcement. Figure 10 compares lateral TSR strains in unconfined (a) and in strengthened specimens (b). Similar trends can be seen between NC and D0_C2 series: there, square-shaped columns record higher lateral stirrup strains in both confined and unconfined cases. Also, in the post-peak branch, TSR strains tend to decrease faster in the circular shape with respect to the squared ones. Figure 11 shows TSR strains (a) and fiber strains (b) for the damaged specimens, showing the same

trend described before about the influence of cross-section geometry on the development of ε_{xx} in the central stirrup.

4.2 Lateral pressure and Fiber-TSR interaction

Generally, confinement effectiveness is considered in concrete confinement models [5, 48-51], whether they are dealing with internally confined (TSR) or externally (FRP, FRCM) confined concrete, through effectiveness coefficients (k_s & k_f). For continuous FRCM jacketing the horizontal efficiency coefficient $k_{f,h}$ depends on the corner radius r and on the cross-section dimensions b and h for rectangular shape, while for circular cross-section this coefficient is assumed to be unitary.

$$k_{f,h} = 1 - \frac{(b-2r)^2+(h-2r)^2}{3bh} \quad (1)$$

Other effectiveness coefficients can be considered to account for fiber orientation with respect to the member axial axis ($k_{f,a}$) or for vertical efficiency in partially wrapped systems ($k_{f,v}$), which are assumed unitary for the analyzed configurations used in this experimental campaign.

For internal confinement by TSR, the geometric effectiveness coefficient does not depend on corner radius but only on the layout and spacing of TSR and can be computed following the Mander et al. approach [48] for circular cross-sections:

$$k_s = \frac{A_e}{(1-\rho_{cc})A_c} = \frac{\left(1-{s'}/{2d_s}\right)^2}{1-\rho_{cc}} \quad (2)$$

and for rectangular ones:

$$k_s = \frac{\left[(1-\sum_{i=1}^{n}\frac{(w_i')^2}{6b_cd_c})(1-\frac{s'}{2b_c})(1-\frac{s'}{2d_c})\right]}{(1-\rho_{cc})} \quad (3)$$

where A_e is the effectively confined concrete area; A_c is the concrete core area; ρ_{cc} is the longitudinal reinforcement ratio to the core area; s' is the clear vertical spacing between consecutive stirrups; d_s is the hoop diameter for circular cross-sections; w_i' is the i-th clear distance between adjacent longitudinal bars; b_c and d_c are the concrete core dimensions taken between stirrups centerlines.

Once the effectiveness coefficients are known, the lateral confining pressure can be computed for both internal TSR:

$$f_{ls} = \frac{1}{2} k_s \rho_{st} \sigma_{st} \quad (4)$$

and external FRCM system:

$$f_{lf} = \frac{1}{2} k_f \rho_f \sigma_f \quad (5)$$

where ρ_{st} and ρ_f are the volumetric ratio of TSR and FRCM and σ_{st} and σ_f are stresses in stirrup and fibers.

For rectangular cross-sections, the confining pressure should be computed separately in the two main directions ($f_{ls,x}$ and $f_{ls,y}$), since for non-symmetrical sections lateral pressure can be different. Mander et al. [48] sets σ_{st} equal to the yielding stress of the reinforcement.

Pellegrino & Modena [5] studied the interaction between internal TSR and external FRP confinement proposing an additive model to compute the overall confining pressure offered by both systems. However, such interaction is not yet studied for FRCM confining systems and existing models generally neglect TSR contribution. The issue is even less clear when it comes to repairing and not just strengthening of existing structures. To investigate this phenomenon, strain data on both fibers and TSR were collected experimentally through electrical strain gages. The experimental data gathered in this campaign suggest that, at least for damaged elements, TSR contribution and fiber-TSR interaction are important factors in the behavior of damaged RC elements repaired through FRCM confinement, since they grow at similar rates both in the pre- and post-peak branches of stress-strain curves.

Fiber and TSR mean strain values for peak and ultimate load are reported in Table 4. Based on these strain values and on the effectiveness coefficients computed as shown in the above equations, confining pressure exerted by TSR and FRCM at peak and ultimate (80%) load was computed and reported in Table 5. Also, the total confining pressure $f_{l,tot}$, computed as the sum of TSR and fiber pressure, is given for peak and ultimate load.

It can be noted that the confining pressure exerted by TSR (f_{ls}) at peak load is almost the same for specimens with the same stirrup spacing regardless of their cross-section. TSR confining pressure is

significantly lower for the S33 geometries than in all other cases. On the other hand, FRCM provides continuous confinement to the columns and is more influenced by cross-section shape than TSR, thus varying more between prismatic and cylinder columns. For damaged and repaired columns, confining pressure at peak load exerted by fibers results similar for S20 and S33 specimens, while the circular one (C20) displays slightly smaller lateral pressure. This value becomes much bigger in the post-peak branch, exceeding largely those values recorded by the specimens with the square cross-section.

In the S33 specimens, FRCM contribution to the overall confinement results significantly higher than the TSR effect. Instead, for 200 mm stirrup spacing, fiber and TSR contribution to the overall confining pressure at peak load becomes similar, even though, a higher TSR effect is seen in the circular section. At the ultimate load, FRCM confining pressure results more than double the TSR pressure in the circular shaped specimens while in the squared one the two pressures result quite comparable. Considering the total confining pressure as a simple addition of the TSR and fiber contributions, the highest value (0.169 MPa) at peak load is recorded in the S20 specimens while for ultimate load in the C20 one (0.688 MPa). In the undamaged specimens, fiber confining pressure resulted in smaller and more dispersive values.

The results in terms of lateral confinement pressure highlight how neglecting the contribution of transverse reinforcement, as existing models on FRCM confinement of concrete currently do, is an assumption that does not reflect the actual behavior, at least for elements with not too large stirrups spacing. In addition, recalling the results in terms of strength enhancement after repair, where the circular-shaped column performed undoubtedly better than the squared-section ones, results show also that a simple additive contribution of the two reinforcements does not well describe the overall behavior and particularly the interaction of the two reinforcements under the axial loading.

5. CONCLUSIONS

The experimental work presented in this paper aimed to study the effectiveness of FRCM systems to adequately repair RC columns through confinement. Two different cross-section shapes (circular and

squared) and two TSR spacing (200 and 330 mm) were considered in full-scale specimens. Results of repaired specimens were then compared to the results of unconfined undamaged specimens and FRCM confined undamaged RC specimens. Hoop strains were monitored in both TSR and fibers to evaluate the effective confining pressure and possible interaction between internal and external confining systems. Based on the experimental results previously discussed, the following conclusions can be drawn:

- repair through CFRCM confinement was able to enhance concrete strength in all considered specimens. Compared to the residual axial capacity of the damaged specimens, the repair protocol was able to enhance concrete strength by a factor of 2.18 in the circular-shaped C20_D1 specimen, 1.75 in the squared-shape S20_D1 and 1.40 in the squared-shape S33_D1 specimen;
- cross-section shape and TSR spacing have an important effect in the overall repair effectiveness. The circular-shaped specimen C20_D1_C2 was able to match the resistance of the undamaged FRCM confined C20_D0_C2 specimen while the squared S20_D1_C2 equaled the undamaged C20_NC resistance. The squared specimen with higher TSR spacing was able to reach only 90% of the S33_NC strength;
- peak and ultimate axial strain did not improve much in all repaired specimens and resulted in lower values with respect to the NC series, apart specimen S33_D1_C2 which stress-strain curve resulted in a slightly different trend with respect to the other two;
- damaged specimens developed lateral strains in TSR and fibers at higher rates than undamaged ones. Higher strain values were recorded in specimens with less effective confining systems due to both section-shape and TSR ratio. Similar trends were noted for TSR and fiber strains in all specimens;
- estimated confining pressure exerted by TSR and FRCM confinement highlights the importance of TSR spacing and the results seems to suggest that a simple additive model of the two contributions (fiber & TSR) might not be the best solution to describe the interaction between the internal and external confining systems.

It is important to emphasize that further research on this issue is needed given the lack of existing studies that experimentally investigate FRCM-TSR interaction in concrete confinement and the limited number of specimens, due to their real scale dimensions, investigated in the present one.

REFERENCES

[1] McGarry, F. J. (1970). Building design with fibre reinforced materials. *Proceedings of the Royal Society of London. A. Mathematical and Physical Sciences*, *319*(1536), 59-68.

[2] Fardis, M. N., & Khalili, H. H. (1982). FRP-encased concrete as a structural material. *Magazine of Concrete Research*, *34*(121), 191-202.

[3] Campione, G., Colajanni, P., La Mendola, L., & Spinella, N. (2007). Ductility of reinforced concrete members externally wrapped with fiber-reinforced polymer sheets. *Journal of Composites for Construction*, 11(3), 279-290.

[4] Mirmiran, A., Shahawy, M., Samaan, M., Echary, H. E., Mastrapa, J. C., & Pico, O. (1998). Effect of column parameters on FRP-confined concrete. *Journal of Composites for Construction*, 2(4), 175-185.

[5] Pellegrino, C., & Modena, C. (2010). Analytical model for FRP confinement of concrete columns with and without internal steel reinforcement. *Journal of Composites for Construction*, 14(6), 693-705.

[6] Realfonzo, R., & Napoli, A. (2011). Concrete confined by FRP systems: confinement efficiency and design strength models. *Composites Part B: Engineering*, 42(4), 736-755.

[7] Saadatmanesh, H., Ehsani, M. R., & Jin, L. (1997). Repair of earthquake-damaged RC columns with FRP wraps. *ACI Structural Journal*, *94*, 206-215.

[8] Li, G., Hedlund, S., Pang, S. S., Alaywan, W., Eggers, J., & Abadie, C. (2003). Repair of damaged RC columns using fast curing FRP composites. *Composites Part B: Engineering*, *34*(3), 261-271.

[9] Faleschini, F., Gonzalez-Libreros, J., Zanini, M. A., Hofer, L., Sneed, L., & Pellegrino, C. (2019). Repair of severely-damaged RC exterior beam-column joints with FRP and FRCM composites. *Composite Structures*, *207*, 352-363.

[10] Eid, R., & Paultre, P. (2008). Analytical model for FRP-confined circular reinforced concrete columns. *Journal of Composites for Construction*, 12(5), 541-552.

[11] Teng, J. G., Lin, G., & Yu, T. (2015). Analysis-oriented stress-strain model for concrete under combined FRP-steel confinement. *Journal of Composites for Construction*, 19(5), 04014084.

[12] Lin, G., Yu, T., & Teng, J. G. (2016). Design-oriented stress–strain model for concrete under combined FRP-steel confinement. *Journal of Composites for Construction*, 20(4), 04015084.

[13] Al-Rahmani, A., & Rasheed, H. (2016). Combined Transverse Steel-External FRP Confinement Model for Rectangular Reinforced Concrete Columns. *Fibers*, 4(1), 8.

[14] Kaeseberg, S., Messerer, D., & Holschemacher, K. (2020). Experimental Study on Concrete under Combined FRP–Steel Confinement. *Materials*, 13(20), 4467.

[15] Bournas, G. Cerniauskas Z. Tetta DA, & Bisby L.A. (2020). Concrete confinement with TRM versus FRP jackets at elevated temperatures. *Materials and Structures 53*: 58.

[16] Lionetto F,, Aiello, M.A., & Maffezzoli, A. (2018). Reversible FRP-confinement of heritage masonry columns. In: *9th International Conference on Fibre-Reinforced Polymer (FRP) Composites in Civil Engineering* (CICE 2018), 2018, Paris 17–19 July 2018.

[17] Zhao, J., & Vokkarane, V.M. (2017). Reverse manycast data retrieval in Elastic Optical Networks, In: *2017 International Conference on Computing, Networking and Communications (ICNC)*, Santa Clara, CA, 2017, pp. 402-407, doi: 10.1109/ICCNC.2017.7876162.

[18] Bencardino, F., Carloni, C., Condello, A., Focacci, F., Napoli, A., & Realfonzo, R. (2018). Flexural behaviour of RC members strengthened with FRCM: State-of-the-art and predictive formulas. *Composites Part B: Engineering*, *148*, 132-148.

[19] Sneed, L. H., Verre, S., Carloni, C., & Ombres, L. (2016). Flexural behavior of RC beams strengthened with steel-FRCM composite. *Engineering Structures*, *127*, 686-699.

[20] Raoof, S. M., Koutas, L. N., & Bournas, D. A. (2017). Textile-reinforced mortar (TRM) versus fibre-reinforced polymers (FRP) in flexural strengthening of RC beams. *Construction and Building Materials*, *151*, 279-291.

[21] El-Sherif, H., Wakjira, T. G., & Ebead, U. (2020). Flexural strengthening of reinforced concrete beams using hybrid near-surface embedded/externally bonded fabric-reinforced cementitious matrix. *Construction and Building Materials*, 238, 117748.

[22] Gonzalez-Libreros, J. H., Sneed, L. H., D'Antino, T., & Pellegrino, C. (2017). Behavior of RC beams strengthened in shear with FRP and FRCM composites. *Engineering Structures*, *150*, 830-842.

[23] Wakjira, T. G., & Ebead, U. (2019). A shear design model for RC beams strengthened with fabric reinforced cementitious matrix. *Engineering Structures*, *200*, 109698.

[24] Triantafillou, T. C., & Papanicolaou, C. G. (2006). Shear strengthening of reinforced concrete members with textile reinforced mortar (TRM) jackets. *Materials and Structures*, 39(1), 93-103.

[25] Mofidi, A., Cheng, L., Chaallal, O., & Shao, Y. (2018). Shear Strengthening of RC Beams with NSM FRP—Influencing Parameters and A Theoretical Model. *ACI Special Publication*, 327, 31-1.

[26] Fossetti, M., Alotta, G., Basone, F., & Macaluso, G. (2017). Simplified analytical models for compressed concrete columns confined by FRP and FRCM system. *Materials and Structures*, *50*(6), 240.

[27] Murgo, F. S., & Mazzotti, C. (2019). Masonry columns strengthened with FRCM system: Numerical and experimental evaluation. *Construction and Building Materials*, 202, 208-222.

[28] Incerti, A., Vasiliu, A., Ferracuti, B., & Mazzotti, C. (2015). Uni-Axial compressive tests on masonry columns confined by FRP and FRCM. In: *Proc. of the 12th International Symposium on Fiber Reinforced Polymers for Reinforced Concrete Structures & The 5th Asia-Pacific Conference on Fiber Reinforced Polymers in Structures, Joint Conference*, Nanjing, China, 14–16 December 2015.

[29] Colajanni, P., Fossetti, M., & Macaluso, G. (2014). Effects of confinement level, cross-section shape and corner radius on the cyclic behavior of CFRCM confined concrete columns. *Construction and Building Materials*, *55*, 379-389.

[30] Ombres, L. (2007). Confinement effectiveness in concrete strengthened with fiber reinforced cement based composite jackets. In: *Proc., FRPRCS-8, 8th Int. Symp. on Fiber Reinforced Polymer Reinforcement for Concrete Structures*, T. C. Triantafillou, ed., Univ. of Patras, Patras, Greece.

[31] Ombres, L. (2014). Concrete confinement with a cement based high strength composite material. *Composite Structures*, *109*, 294-304.

[32] Ombres, L., & Mazzuca, S. (2017). Confined concrete elements with cement-based composites: confinement effectiveness and prediction models. *Journal of Composites for Construction*, 21(3), 04016103.

[33] Triantafillou, T. C., Papanicolaou, C. G., Zissimopoulos, P., & Laourdekis, T. (2006). Concrete confinement with textile-reinforced mortar jackets. *ACI Materials Journal*, 103(1), 28.

[34] Gonzalez-Libreros, J., Zanini, M. A., Faleschini, F., & Pellegrino, C. (2019). Confinement of low-strength concrete with fiber reinforced cementitious matrix (FRCM) composites. *Composites Part B: Engineering*, 177, 107407.

[35] Bournas, D. A., Lontou, P. V., Papanicolaou, C. G., & Triantafillou, T. C. (2007). Textile-reinforced mortar versus fiber-reinforced polymer confinement in reinforced concrete columns. *ACI Structural Journal*, 104(6), 740.

[36] Faleschini, F., Zanini, M. A., Hofer, L., & Pellegrino, C. (2020). Experimental behavior of reinforced concrete columns confined with carbon-FRCM composites. *Construction and Building Materials*, *243*, 118296.

[37] Faleschini, F., Zanini, M. A., Hofer, L., Toska, K., De Domenico, D., & Pellegrino, C. (2020). Confinement of reinforced concrete columns with glass fiber reinforced cementitious matrix jackets. *Engineering Structures*, *218*, 110847.

[38] Peled, A. (2007). Confinement of damaged and nondamaged structural concrete with FRP and TRC sleeves. *Journal of Composites for Construction*, *11*(5), 514-522.

[39] Gonzalez-Libreros, J., Sabau, C., Sneed, L. H., Sas, G., & Pellegrino, C. (2017, September). Effect of confinement with FRCM composites on damaged concrete cylinders. In *International Conference on Strain-Hardening Cement-Based Composites* (pp. 770-777). Springer, Dordrecht.

[40] EN 206 (2013). Concrete. Specification, performance, production and conformity. European Committee for standardization, Brussels, Belgium.

[41] EN 1015-11 (2019). Methods of test for mortar for masonry. Determination of flexural and compressive strength of hardened mortar. European Committee for standardization, Brussels, Belgium.

[42] Chellapandian, M., Prakash, S. S., & Sharma, A. (2019). Axial compression–bending interaction behavior of severely damaged RC columns rapid repaired and strengthened using hybrid FRP composites. *Construction and Building Materials*, 195, 390-404.

[43] He, R., Sneed, L. H., & Belarbi, A. (2013). Rapid repair of severely damaged RC columns with different damage conditions: An experimental study. *International Journal of Concrete Structures and Materials*, 7(1), 35-50.

[44] Ombres, L. (2015). Analysis of the bond between fabric reinforced cementitious mortar (FRCM) strengthening systems and concrete. *Composites Part B*: Engineering, 69, 418-426.

[45] D'Ambrisi, A., Feo, L., & Focacci, F. (2012). Bond-slip relations for PBO-FRCM materials externally bonded to concrete. *Composites Part B*: Engineering, 43(8), 2938-2949.

[46] Caggegi, C., Sciuto, D., & Cuomo, M. (2018). Experimental study on effective bond length of basalt textile reinforced mortar strengthening system: Contributions of digital image correlation. *Measurement*, 129, 119-127.

[47] Raoof, S. M., Koutas, L. N., & Bournas, D. A. (2016). Bond between textile-reinforced mortar (TRM) and concrete substrates: Experimental investigation. *Composites Part B*: Engineering, 98, 350-361.

[48] Mander, J. B., Priestley, M. J., & Park, R. (1988). Theoretical stress-strain model for confined concrete. *Journal of Structural Engineering*, 114(8), 1804-1826.

[49] Spoelstra, M. R., & Monti, G. (1999). FRP-confined concrete model. *Journal of composites for construction*, 3(3), 143-150.

[50] Bisby, L. A., Dent, A. J., & Green, M. F. (2005). Comparison of confinement models for FRP wrapped concrete. *ACI Structural Journal*, 62-72.

[51] Lam, L., & Teng, J. G. (2003). Design-oriented stress–strain model for FRP-confined concrete. *Construction and Building Materials*, 17(6-7), 471-489.

TABLES

Table 1. Specimens characteristics.

Specimen ID	Geometry			Steel Reinforcement *B450C*		Concrete		FRCM Confinement	
	Section geometry	Specimen dimensions (mm)	Corner radius	A_{sl} (mm^2)	A_{sw} (mm^2/m)	Concrete batch f_{cm} (MPa)	Concrete Damage	Presence	Number of layers
C20_NC	cylinder	d = 300; h = 1000	-	615	502	17.4	-	no	-
S20_NC	square	l = 300; h = 1000	20	615	502	17.4	-	no	-
S33_NC	square	l = 300; h = 1000	20	615	301	24.1	-	no	-
C20_D0_C2	cylinder	d = 300; h = 1000	-	615	502	17.4	-	yes	2
S20_D0_C2	square	l = 300; h = 1000	20	615	502	17.4	-	yes	2
S33_D0_C2	square	l = 300; h = 1000	20	615	301	24.1	-	yes	2
C20_D1_C2	cylinder	d = 300; h = 1000	-	615	502	17.4	yes, 70%	yes	2
S20_D1_C2	square	l = 300; h = 1000	20	615	502	17.4	yes, 70%	yes	2
S33_D1_C2	square	l = 300; h = 1000	20	615	301	24.1	yes, 70%	yes	2

Table 2. FRCM and repair mortar properties

Specimen ID	FRCM mortar			Repair mortar		
	ρ (kg/m^3)	f_{cm} (MPa)	$f_{cm,f}$ (MPa)	ρ (kg/m^3)	f_{cm} (MPa)	$f_{cm,f}$ (MPa)
C20_D0_C2	1880 ± 22	30.88 ± 0.78	5.08 ± 0.27	-	-	-
S20_D0_C2	1877 ± 12	32.14 ± 0.62	6.12 ± 0.94	-	-	-
S33_D0_C2	1947 ± 11	33.56 ± 1.81	5.50 ± 1.06	-	-	-
C20_D1_C2	2046 ± 34	21.06 ± 1.39	4.96 ± 0.26	2153 ± 5	22.81 ± 3.76	5.93 ± 0.27
S20_D1_C2	2114 ± 48	23.22 ± 1.62	4.77 ± 0.37	2143 ± 40	21.58 ± 1.59	5.08 ± 0.36
S33_D1_C2	2047 ± 19	20.71 ± 1.16	4.92 ± 0.43	2091 ± 78	28.20 ± 2.30	5.41 ± 0.90

Table 3. Specimens test results

Specimen ID	$f_{c0(cc)}$ [MPa]	$f_{cu(ccu)}$ [MPa]	$f_{u,D}$ [MPa]	$e_{c0(cc)}$ [-]	$e_{cu(ccu)}$ [-]	f_{cc}/f_{c0} [-]	f_{ccu}/f_{cu} [-]	e_{cc}/e_{c0} [-]	e_{ccu}/e_{cu} [-]	$f_{cc}/f_{u,D}$ [-]
C20_NC	13.15	9.62	8.08	0.0029	0.0065	-	-	-	-	-
S20_NC	14.20	10.58	8.38	0.0018	0.0054	-	-	-	-	-
S33_NC	16.58	12.52	10.68	0.0020	0.0040	-	-	-	-	-
C20_D0_C2	17.63	13.21	-	0.0037	0.0072	1.34	1.376	1.276	1.107	-
S20_D0_C2	14.34	10.71	-	0.0022	0.0070	1.01	1.012	1.222	1.296	-
S33_D0_C2	21.09	16.43	-	0.0022	0.0037	1.27	1.312	1.100	0.925	-
C20_D1_C2	17.62	13.02	-	0.0019	0.0050	1.34	1.353	0.655	0.770	2.180
S20_D1_C2	14.67	10.20	-	0.0014	0.0040	1.03	0.964	0.777	0.741	1.750
S33_D1_C2	14.98	12.05	-	0.0022	0.0046	0.90	0.962	1.100	1.150	1.402

Table 4. Mean TSR and fiber hoop strains at peak and ultimate stress

Specimen ID	$\varepsilon_{s,xx\ (peak)}$ [‰]	$\varepsilon_{s,xx\ (ultimate)}$ [‰]	$\varepsilon_{f,xx\ (peak)}$ [‰]	$\varepsilon_{f,xx\ (ultimate)}$ [‰]
C20_NC	0.0877	0.3585	-	-
S20_NC	0.1762	1.1826	-	-
S33_NC	0.6764	2.3388	-	-
C20_D0_C2	0.1073	0.1646	0.2172	0.2805
S20_D0_C2	0.1971	1.3880	0.1264	0.4285
S33_D0_C2	0.3258	1.7170	0.2520	0.6281
C20_D1_C2	0.5070	1.2074	0.4017	3.2342
S20_D1_C2	1.1069	2.3229	1.0629	2.0963
S33_D1_C2	1.5811	2.3113	1.1363	2.3398

Table 5. Confining pressure exerted from CFRCM and TSR

					peak			ultimate		
Specimen ID	ρ_s	k_s	ρ_f	k_f	f_{ls} [MPa]	f_{lf} [MPa]	$f_{l,tot}$ [MPa]	f_{ls} [MPa]	f_{lf} [MPa]	$f_{l,tot}$ [MPa]
C20_NC	0.00387	0.403	-	-	0.014	-	0.014	0.059	-	0.059
S20_NC	0.00387	0.197	-	-	0.014	-	0.014	0.095	-	0.095
S33_NC	0.00234	0.067	-	-	0.009	-	0.009	0.038	-	0.038
C20_D0_C2	0.00387	0.403	0.00125	1.000	0.018	0.033	0.050	0.027	0.043	0.069
S20_D0_C2	0.00387	0.197	0.00125	0.499	0.016	0.010	0.025	0.111	0.032	0.144
S33_D0_C2	0.00234	0.067	0.00125	0.499	0.005	0.019	0.024	0.028	0.048	0.076
C20_D1_C2	0.00387	0.403	0.00125	1.000	0.083	0.061	0.144	0.197	0.490	0.688
S20_D1_C2	0.00387	0.197	0.00125	0.499	0.089	0.080	0.169	0.186	0.159	0.345
S33_D1_C2	0.00234	0.067	0.00125	0.499	0.026	0.086	0.112	0.038	0.177	0.215

FIGURES

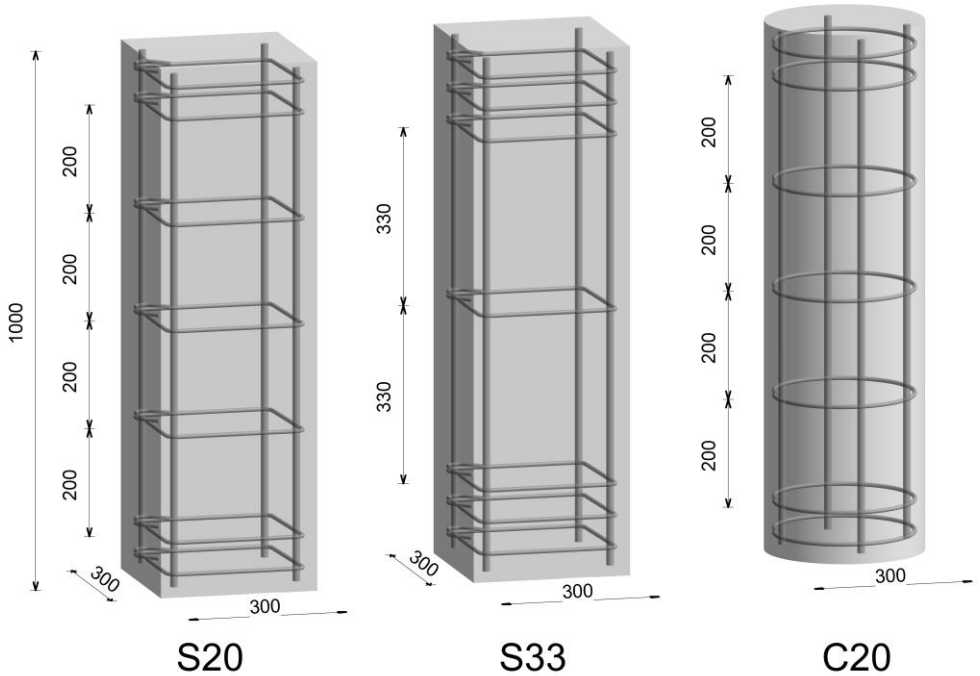

Figure 1. Reinforcement details.

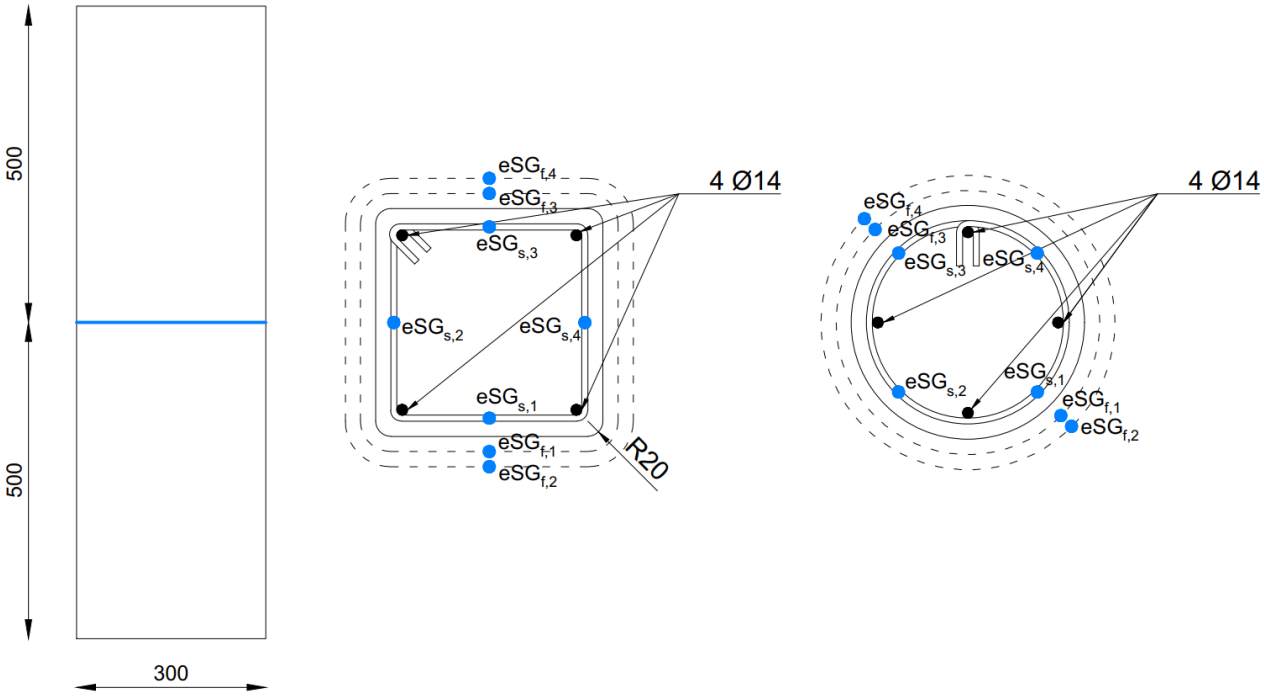

Figure 2. Disposition of eSGs to evaluate stirrup and fibers strains.

Figure 3. S33_NC specimen after failure (a); S33_NC specimen after repair operation (b).

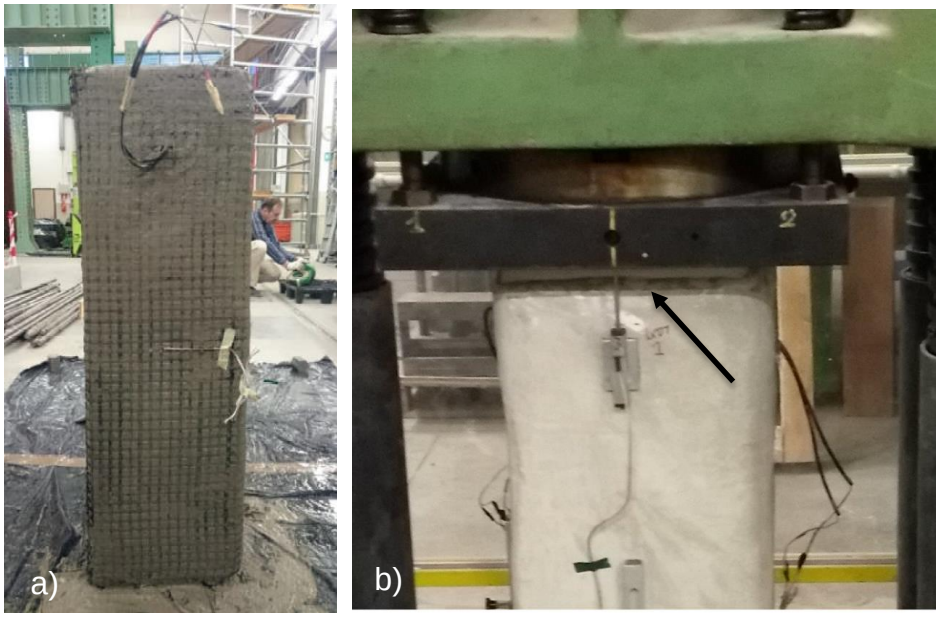

Figure 4. Application of the first FRCM layer onto the S33_D1_C2 specimen (a); detail of the top of S33_D1_C2 specimen prior to the test (b).

Figure 5. C20_NC, C20_D0_C2 and C20_D1_C2 at the end of the loading history

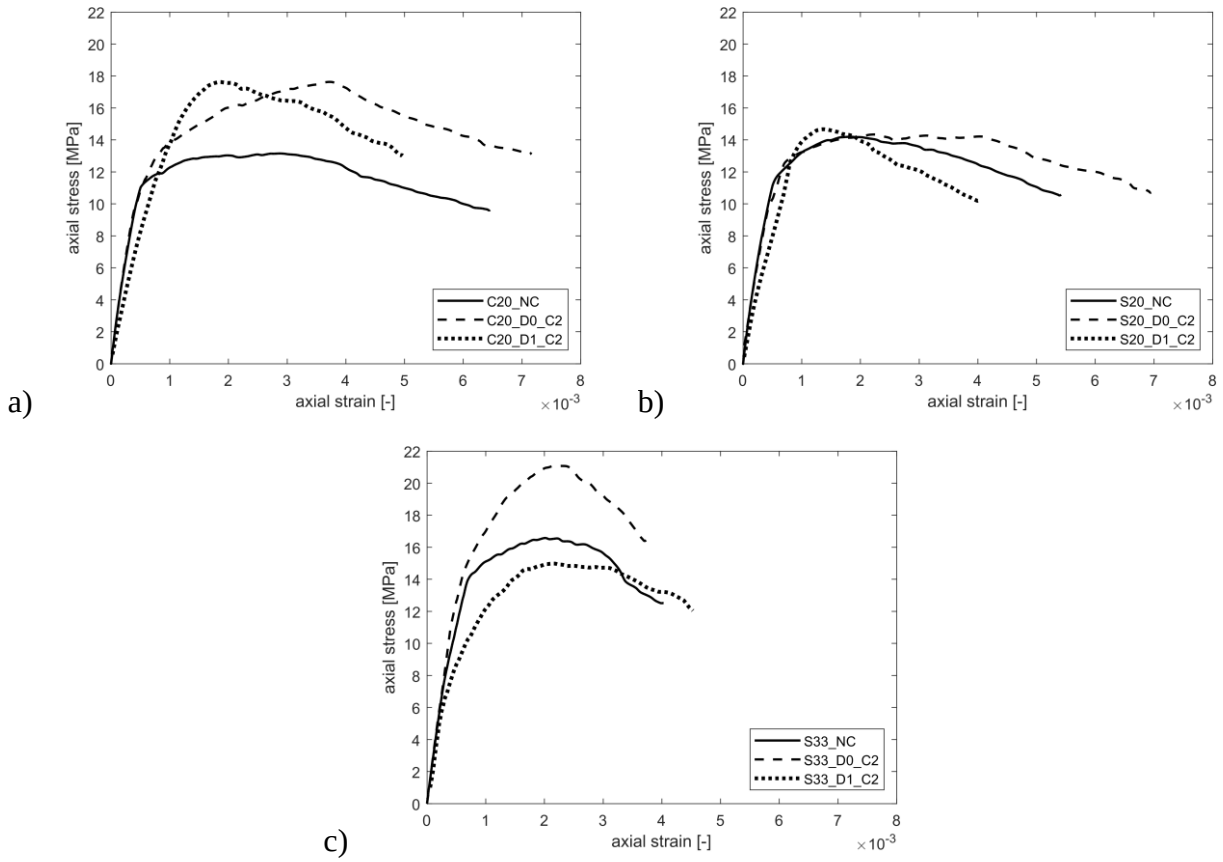

Figure 6. Axial stress strain behavior of the considered unconfined (NC), undamaged strengthened (D0) and damaged repaired (D1) specimens.

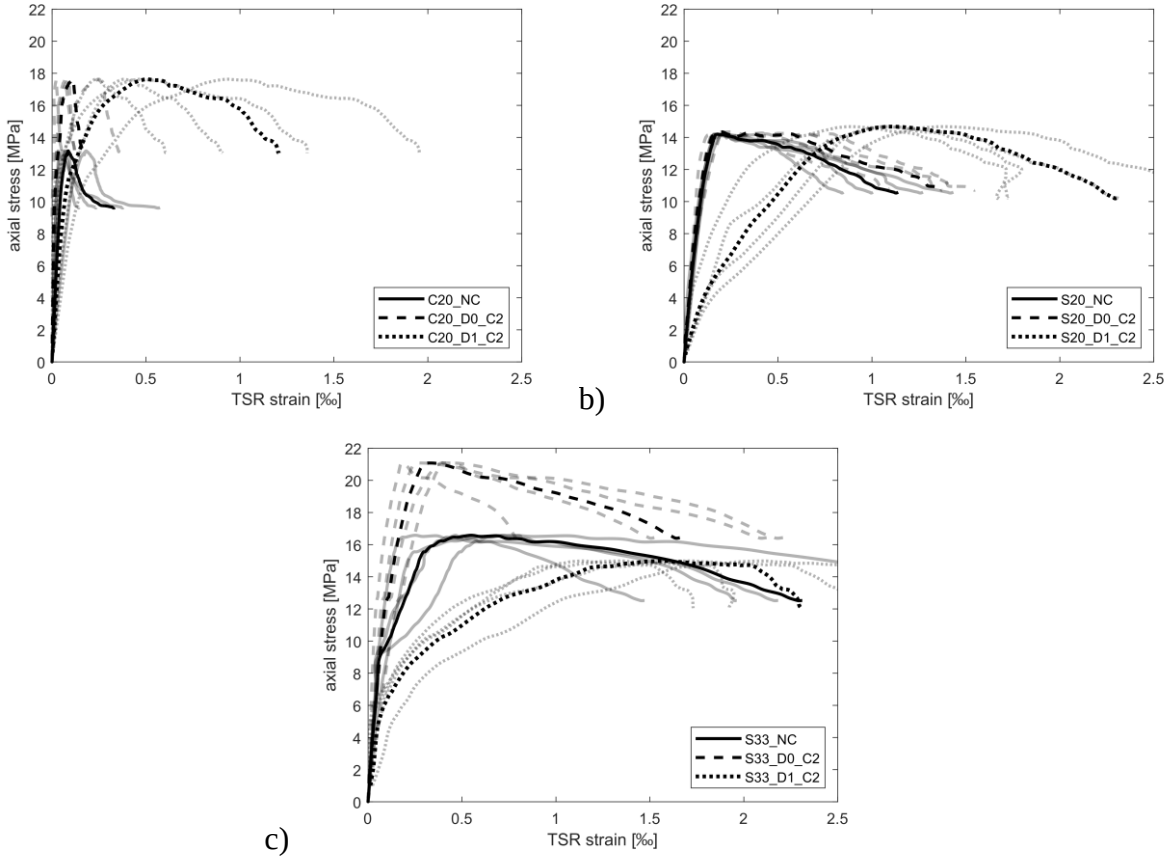

Figure 7. Axial stress – TSR strains for unconfined, undamaged strengthened and damaged repaired columns. (a) C20, b) S20 and c) S_33 specimens

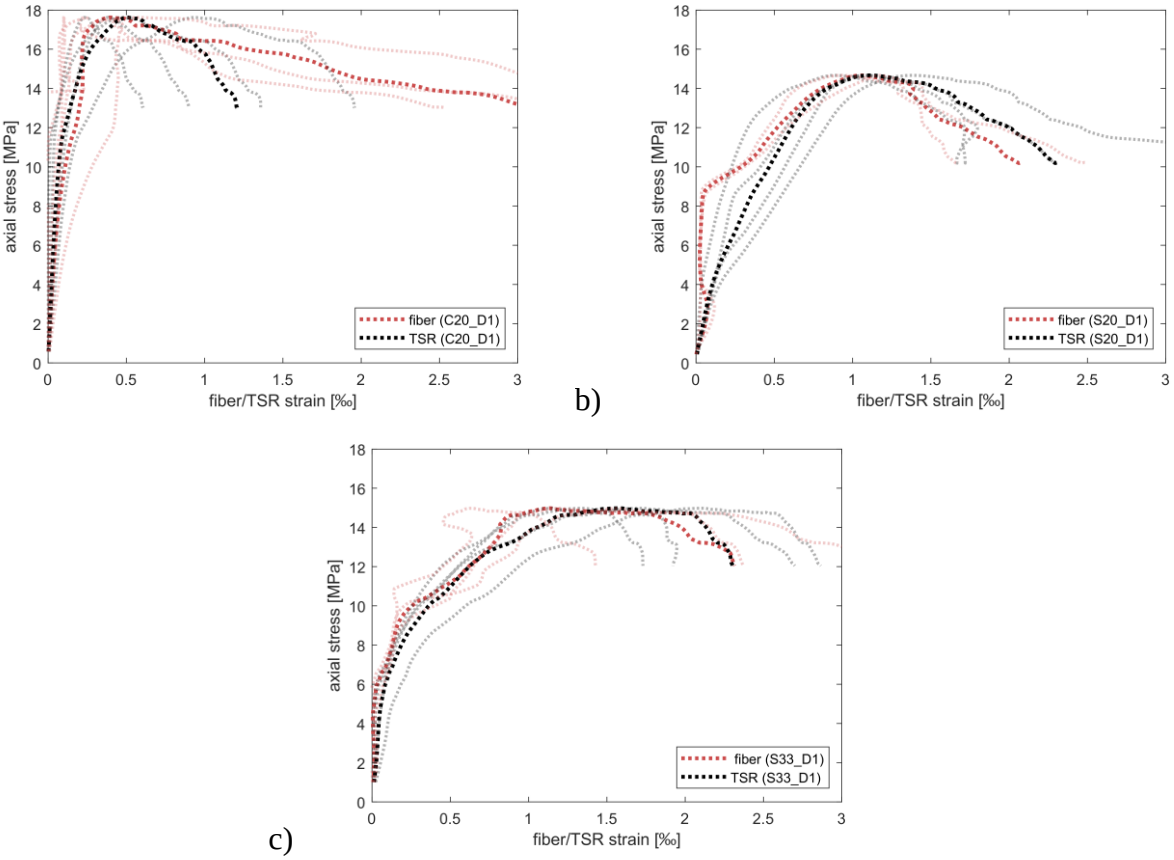

Figure 8. Axial stress – fiber and TSR strain for damaged repaired specimens. a) C20_D1_C2, b) S20_D1_C2, c) S33_D1_C2

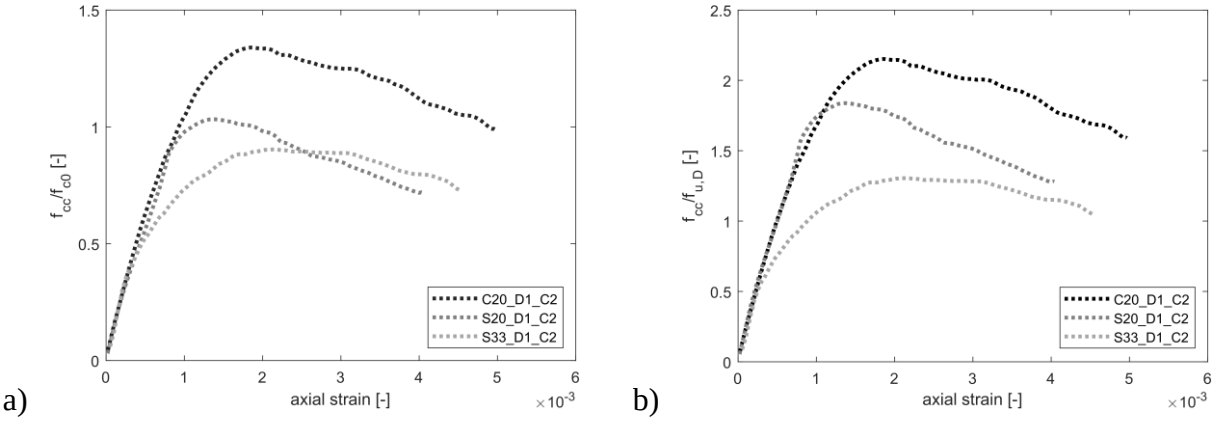

a) b)

Figure 9. Relative axial stress – strain curve with respect to the undamaged cases (a) and to the residual axial capacity of the damaged specimens (b).

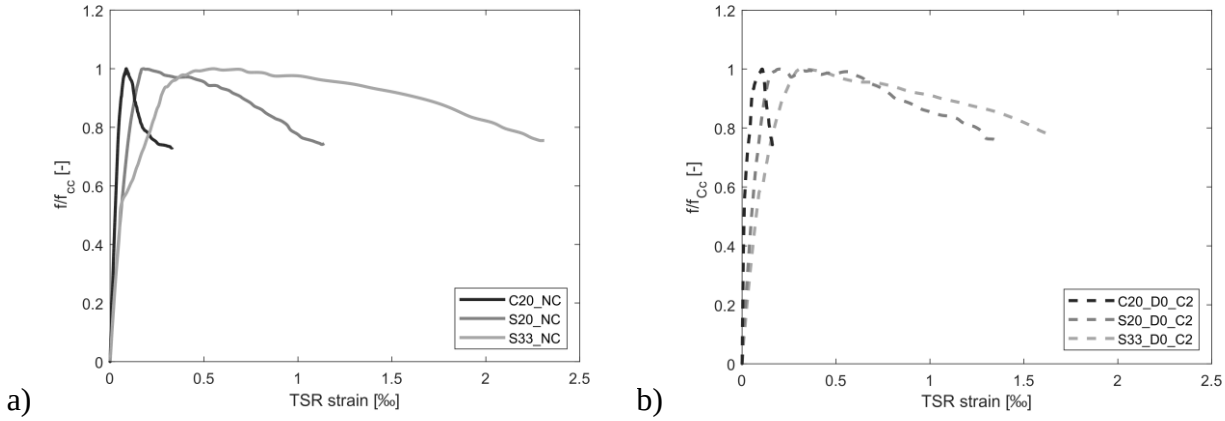

a) b)

Figure 10. TSR strains in unconfined (a) and in undamaged strengthened specimens (b)

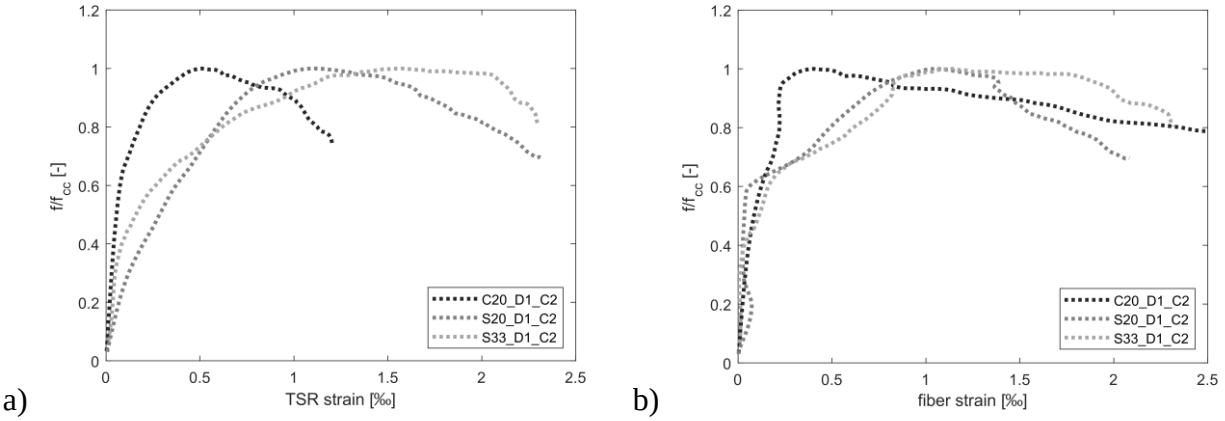

a) b)

Figure 11. TSR (a) and fiber (b) strains in the damaged repaired specimens

Reviewers' comments:

Reviewer #1:

> The paper describes the results of an experimental investigation on the behavior of severely damaged reinforced concrete columns confined with FRCM. Nine reinforced concrete columns were tested and the influence of the shape effect and transverse steel reinforcement -fiber interaction was analyzed. The subject matter of the paper is actual and fits well with the scope of the Journal. The text is well written and organized: the experimental results were accurately discussed, The paper can be accepted for its publication in the Journal after the following minor revisions :

The authors gratefully thank the referee for the comments and suggestions provided, which allowed us to improve the quality of the manuscript.

> the Authors are requested to clarify why the confinement was made using two layer of carbon fabrics (why two instead of one);

The fabric used for the repairing was relatively light weighted (170g/m) and based on the authors experience a single layer would have been too little to adequately confine the real scale RC columns analyzed in this study. Further, this choice was motivated based on a previous experimental campaign carried out by some of the authors where they used the same fabric type to confine bare concrete cylinders, obtaining strength enhance between 10 and 20% with 2 layers (see ref 39). This has been motivated in the text at lines 157-160.

> it is suggested to report in the text the number of specimen tested to determine the mechanical properties of the FRCM system (lines 146-147);

Three specimens were tested to determine the mechanical properties of the system. The information was added to the paper at lines 165-166.

> it is needed to justify why an overlap length of 200 mm was used;

An overlapping of 200mm was used based on a literature review on the bond between FRCM systems and concrete substrates. Ombres (2015) and D'Ambrisi (2012) reported an effective bond length ranging between 150mm and 200mm in PBO FRCM – Concrete systems; Caggegi et al. (2018) reported an effective bond length related to Basalt TRM strengthening system of approximately 125 mm with an experimental study; Raof et al. (2016) found that the effective bond length is in the range of 200-300 mm depending on the examined number of layers used with carbon fabric. This information is added in the text at lines 216-221. Four new references were added (see refs. 44-47). However, the authors recognize that varying this parameter may have an effect on the confinement provided by the composite; this effect will be studied in a further experimental campaign on small-scale specimens, which allows to test more samples to better address the influence of this variable.

> to validate the last Conclusion "the estimated confining pressure exerted by the transversal steel reinforcement (TSR) and the FRCM confinement ... suggest that a simple additive model of the two contributions (fiber and TSR) is not the best solution to describe the interaction between the internal and external confining system" it is suggested to analyze further experimental results available in the literature.

The authors agree with the referee who addresses the need to find further experimental results in literature, because this experimental campaign presents a limited number of specimens. The conclusion has been rephrased in the text (see lines 510-513). Also, a paragraph highlighting the aforementioned limit was added in the conclusion section (see lines 514-516).

Recall, however, that only few studies have already analyzed the interaction of FRCM and TSR confinement, because experimental campaigns were rarely devoted to test real scale specimens with both inner and external confining system. Almost none experimentally investigates strain development in both TSR and FRCM confining systems, and in none of them damaged specimens were analyzed. Hence, this conclusion, which is

specifically referred to the damaged specimens, could only suggest to improve the number of available specimens to provide a reliable model that describe the interaction between the two confining systems.

Reviewer #2:

> This manuscript presents the results of an experimental program on RC columns repaired through FRCM composites. The effect of pre-damage was investigated but not in-depth (only three columns with pre-damage were tested). I have the following comments which I think the authors should address:

The authors would like to thank the referee for the comments. Concerning the limited amount of specimens tested in this experimental campaign, the referee correctly reports that only three columns were tested with a pre-damage. This number, even if limited, allows us to provide some important conclusions on the effect of using FRCM jackets to repair pre-damaged real-scale columns, which have never been tested before in literature. Further, as an element of novelty, a detailed analysis of strains development both in the inner stirrups and in the fibers has been provided. It is worth recalling that, when dealing with almost real-scale elements, the number of tested elements is always more limited than when dealing with small scale cylinders, made with concrete only and no internal reinforcement, because of the higher economical effort required in such experimental works. The authors hope that the referee can understand the great effort provided for realizing this experimental campaign.

> 1. Table 1: the Asw values are the same for S20 and S33 specimens. Please check. Also, there is one specimen with a length of 350 mm. Please explain.

The incoherent values were due to typo errors and were corrected. See Table 1.

> 2. Only three specimens with pre-damage were tested while the test results seem scattering (Figure 6). Please give justification on how representative these three specimens are and how conclusive are the test results.

One of the limits of the present study is the reduced number of specimens tested, which is always a problem when dealing with real scale specimens. This limit was also highlighted in the conclusion sections (see added lines 514-516). The scattering effect is due to the S20_D0_C2 specimen, which unfortunately, due to compaction / curing problems, showed incoherent results. However, the results are less scattering when comparing unconfined and repaired specimens. An explanation of this result has been added in the results section, at lines 262-269.

> 3. Figure 6: Please explain more why specimen S33_D0_C2 had much higher capacity than the other two specimens, while another story happens in S20 series specimens. Please also explain how the axial stresses were obtained from the test data.

Due to lab limits, two different concrete batches were used to cast the specimens (see Table 1). The concrete batch strength used for the S33 specimens was higher than the batch used for the C20 and S20 specimens. That is why the S33 (in absolute terms) seems to have a much higher capacity than the other two. In relative terms (fcc/fc0) the gain in the S33_D0_C2 specimen is less than the gain in the C20_D0_C2 specimens (see Table 3).
As highlighted in the results section (see Lines 263-269), the S20_D0_C2 unfortunately showed incoherent results which is believed to be due to differences in concrete compaction and curing, leading to a lower strength of the concrete in the S20_D0_C2 specimens with respect to the S20_D0_NC one, even though, the same batch was used in both cases. Also, lower fiber strains were recorded at concrete peak strain for this specimen with respect to the S33_D0_C2 and C20_D0_C2 ones.

The results of the S20_D0_C2 test was still included in the paper for completeness but as specified in the text only the S20_D1_C2 and S20_D0_NC have directly confrontable results since the same specimen (repaired and not) is used. See added text at Lines 153-154.

Axial stresses were computed simply deducing the load beared by the longitudinal bars from the load recorded by the 6MN load cell mounted in the testing machine and then dividing it by the section area of the specimen. This has been added in the text at lines 255-257.

> 4. The authors ignored some important publications on "concrete under combined FRP-steel confinement". Please do a literature review and cite more references.

More references on the topic were included in the paper. See new references [10-14]. Further, a new section is added in the Introduction, see Lines 48-61.

HIGHLIGHTS

- FRCM is used to strengthen and repair RC columns;
- Specimens consist in undamaged and severely damaged RC columns;
- Transverse steel reinforcement and fiber hoop strains are monitored experimentally;
- Repair effectiveness depend on cross-section shape, TSR spacing and damage presence;
- The overall confining pressure exerted by TSR and FRCM is analyzed.

Declaration of interests

☒ The authors declare that they have no known competing financial interests or personal relationships that could have appeared to influence the work reported in this paper.

☐The authors declare the following financial interests/personal relationships which may be considered as potential competing interests:

CRediT author statement:

Klajdi Toska: investigation; formal analysis; methodology; writing (original draft and revision);

Flora Faleschini: conceptualization, methodology, investigation, formal analysis, writing (original draft and revision), supervision.

Mariano Angelo Zanini: conceptualization, methodology, investigation.

Lorenzo Hofer: investigation.

Carlo Pellegrino: funding acquisition; supervision.

REPAIR OF SEVERELY DAMAGED RC COLUMNS THROUGH FRCM COMPOSITES

Authors information:

Klajdi Toska, Department of Civil, Environmental and Architectural Engineering, University of Padova, via Francesco Marzolo 9, Padova, Italy. email: klajdi.toska@dicea.unipd.it

Flora Faleschini, Department of Civil, Environmental and Architectural Engineering, University of Padova, via Francesco Marzolo 9, Padova, Italy. email: flora.faleschini@dicea.unipd.it. *Corresponding author.*

Mariano Angelo Zanini, Department of Civil, Environmental and Architectural Engineering, University of Padova, via Francesco Marzolo 9, Padova, Italy. email: marianoangelo.zanini@dicea.unipd.it

Lorenzo Hofer, Department of Civil, Environmental and Architectural Engineering, University of Padova, via Francesco Marzolo 9, Padova, Italy. email: lorenzo.hofer@dicea.unipd.it

Carlo Pellegrino, Department of Civil, Environmental and Architectural Engineering, University of Padova, via Francesco Marzolo 9, Padova, Italy. email: carlo.pellegrino@unipd.it

REPAIR OF SEVERELY DAMAGED RC COLUMNS THROUGH FRCM COMPOSITES

Klajdi Toska[1], Flora Faleschini[1,*], Mariano Angelo Zanini[1], Lorenzo Hofer[1] and Carlo Pellegrino[1]

[1] Department of Civil, Environmental and Architectural Engineering, University of Padova, via Francesco Marzolo 9, Padova, Italy.

[*] corresponding author: flora.faleschini@dicea.unipd.it

ABSTRACT

This study presents the results of an experimental campaign aimed at testing the effectiveness of carbon fiber reinforced cementitious matrix (CFRCM) confinement as a repair technique for severely damaged reinforced concrete (RC) columns. To evaluate shape effect and transverse steel reinforcement (TSR) – fiber interaction, two different cross-section shapes, and two TSR rates were investigated. Nine full-scale specimens were analyzed considering three control ones, three undamaged specimens confined with two CFRCM layers, and three severely damaged specimens repaired through confinement by two CFRCM layers. Axial stress-strain curves were analyzed to derive strength and ductility enhancement. Finally, TSR and fiber strains were monitored to better comprehend the contributions of internal and external reinforcement to the overall confinement and possible TSR-FRCM interaction.

Keywords: composites, concrete damage, confinement, interaction, FRCM, Repair, RC columns.

1. INTRODUCTION

Composites are now common materials in retrofitting existing under-designed reinforced concrete (RC) structures. The use of Fiber Reinforced systems has been on the focus of many studies since the early 70s even though a broad use of the technique started much later [1,2]. Until lately, composite materials used for rehabilitation of concrete or masonry structures were generally applied through organic matrix (epoxy-based), guaranteeing a significant improvement for both resistance and ductility properties of the strengthened element.

Confinement is one of the main techniques used to retrofit axially loaded elements. Fiber Reinforced polymer (FRP) systems permit to easily confine existing RC elements by wrapping continuously or partially FRP strips, enhancing their axial strength and ductility without a significant increase in weight or lateral stiffness [3-6]. Confinement by FRP systems has proven to be effective also for repairing RC elements damaged due to excessive axial loading or seismic events. Several research works have been carried out to investigate repair effectiveness of FRP confinement both on plain and reinforced concrete. Saadatmanesh et al. [7] investigated the effectiveness of repairing earthquake-damaged RC columns with FRP wraps. Four different specimens were tested under lateral cyclic loading to simulate the seismic effect on the elements, which were then repaired through FRP wraps and re-tested under the same protocol. In general, all repaired specimens performed well under the cyclic loading test, showing an increase in lateral strength varying from 1 to 38%. Li et al. [8] conducted an experimental campaign on 24 RC specimens tested under uniaxial compression that were formerly damaged through split tensile tests. On the other hand, Faleschini et al. [9] investigated experimentally the effectiveness of FRP composites to repair severely-damaged exterior RC beam-column joints, verifying also the contribution of the FRP system on the overall shear capacity of the joints through some analytical models. Some researchers have also experimentally investigated the effect of the combined FRP-steel confinement on the behavior of concrete columns. Eid & Paultre [10] presented a designed-oriented confinement model for assessing the axial and lateral behavior of circular concrete columns confined with steel ties, FRP composites, and both of them. Teng et al.

[11] proposed a stress-strain model for concrete under combined confinement from FRP and TSR, which has been derived in two alternative versions seeking for increasing accuracy of the prediction. Subsequently, Lin et al. [12] presented a design-oriented stress-strain model for concrete under the combined FRP-steel confinement for circular RC columns, showing a good balance between accuracy of the prevision and simplicity of form. Al-Rahmani & Rasheed [13] proposed a confinement model for combined external FRP – internal TSR confinement for rectangular RC columns. Lately, Kaeseberg et al. [14] conducted an extensive experimental research on 63 CFRP-confined plain concrete columns and 60 CFRP-TSR confined specimens, analyzing the influence on the confinement efficiency of different parameters. Finally, a modified stress-strain and ultimate condition design model was proposed.

However, the use of epoxy resins brings some important liabilities to FRP systems. Poor fire resistance [15], difficult application on wet surfaces, low breathability of the substrate, low reversibility [16], and high sensitivity to UV radiations [17] have led to a lower use of FRP systems in favor to new, more compatible and durable solutions. A similar but alternative solution was born from replacing the organic (epoxy) matrix with inorganic cement-based one, generally known as Fiber Reinforced Cementitious Mortar (FRCM) or Textile Reinforced Mortars (TRM). Like FRP systems, FRCMs have been broadly used lately to enhance flexural [18-21] and shear [22-25] strength of beam elements and to enhance axial strength and ductility of concrete or masonry columns through confinement [26-33].

Concrete confinement through FRCM systems has been the subject of many experimental campaigns and research activities. Tests are mainly based on small-scale non-reinforced elements. Triantafillou et al. [33] were one of the first to analyze the effectiveness of confinement through TRM with respect to the more consolidated FRP systems. Results proved that TRM jackets provided a significant increase in strength and ductility to plain concrete specimens, even though this solution resulted slightly less effective than the FRP counterpart. More recently, Colajanni et al. [29] analyzed the effect of fiber ratio, cross-section shape and corner radius in FRCM confined specimens tested under

monotonic and cyclic axial loading. Ombres et al. conducted several experimental campaigns [30-31] on small-scale plain concrete specimens confined with FRCM systems and later proposed a prediction model based on experimental data collected from different research works [32]. Gonzalez-Libreros et al. [34] also analyzed confinement of plain concrete specimens using CFRCM and GFRCM (the former with carbon, and the latter with glass fibers). The investigation included also the monitoring of hoop strains developed on fibers, to better understand the influence of fiber properties on the FRCM confinement effectiveness. The study showed that fiber exploitation ratio and final confinement effectiveness strongly depends on fabric properties used in the FRCM system. On the other hand, less experimental work can be found on FRCM confinement of real-scale reinforced concrete elements. Bournas et al. [35] investigated confinement effectiveness of FRCM on small-scale RC specimens tested under uniaxial compression loading and on nearly full-scale RC columns tested under cyclic lateral loading. Results showed that FRCM jacketing effectiveness was similar to that of specimens confined with FRPs even though a slight difference of nearly 10% was observed on the uniaxial compressive tests. Recently, some of the authors have investigated confinement effectiveness of FRCM systems on full-scale RC columns comparing different cross-section shapes and steel reinforcement configurations using carbon fibers [36] and glass fibers [37]. Both studies investigated strain development both on transverse steel reinforcement and on confining fibers to evaluate the influence of the axial rigidity of the composites on the effectiveness of the FRCM system and the interaction between internal transverse steel reinforcement and the external FRCM confinement.

While FRCM systems have proven to confer an adequate level of confinement to existing concrete elements, little work has been done to evaluate their effectiveness in the repair of damaged RC elements by excessive axial loads or, as often happens, by seismic loads. Few studies have been carried out on small-scale plain concrete specimens, worth mentioning Peled [38] who studied confinement of damaged and undamaged concrete elements with FRP and FRCM systems. Results showed that composite systems were able to provide an adequate enhancement of axial strength and

ductility even for specimens with initial damage conditions. The effectiveness was observed also by Gonzalez-Libreros et al. [39], where small-scale plain concrete specimens were initially damaged through post-peak compressive loading, then confined by CFRCM and re-tested under monotonic axial load. Results showed that CFRCM confinement was able to restore the original axial capacity of the specimens.

However, on the best authors' knowledge, the few experimental works cited above on the effectiveness of FRCM jackets on damaged axially-loaded columns dealt only with small scale specimens, and considered only plain concrete (without any internal reinforcement). The present paper's goal is to investigate the effectiveness of CFRCM composites to adequately repair severely damaged RC columns. The experimental campaign considers different cross-section shapes (circular and squared), different internal reinforcement configurations and compares the results of unconfined RC members, CFRM confined specimens with undamaged conditions (strengthened) and CFRCM confined specimens with severe damage conditions (severely-damaged and repaired). In addition, hoop strains of transverse steel reinforcement (TSR) and external fiber reinforcement have been investigated to better understand fiber exploitation and steel-fiber interaction in specimens with different initial conditions.

2. MATERIALS AND EXPERIMENTAL PROGRAM

2.1 Test specimens

The research program deals with the study of nine RC samples, which differ by the following variables: cross-section shape; inner transverse reinforcement amount; concrete damage presence or not; presence of FRCM jacket or not. Specimens' main features are described in Table 1. Overall, it is possible to classify them in three main categories: unconfined; strengthened; severely-damaged and repaired.

All the columns present the same height h = 1000 mm and concrete cover c = 20 mm. Two cross-section geometries are investigated, a circular one *C* with diameter d = 300 mm; and a squared one *S*

with size l = 300 mm. In this latter case, the same corner radius r of 20 mm was used in all the prismatic columns. Concerning the inner reinforcement, details are shown in Figure 1: there, it is possible to observe how for all the test specimens the same longitudinal steel reinforcement (A_{sl}) is adopted, consisting in four 14-mm diameter bars, equally spaced in the cylinders and placed at section edges in the prisms. Conversely, the amount of TSR (A_{sw}) varies adopting two configurations. Cylinders present only one single TSR type, consisting in circular hoops with 8-mm diameter bars, placed each 200 mm in the central part of the specimen. Two legged stirrups with 8-mm diameter bars are used instead in prismatic specimens, adopting two spacings in central region of the columns, namely 200 and 330 mm. Steel reinforcement bar properties were the same for all the configurations, and they were experimentally evaluated on three specimens per each type through tensile tests, being f_y = 552 ± 10 MPa at ε_y = 0.002, f_t = 650 ± 15 MPa at ε_t = 0.090 for the longitudinal 14-mm diameter bars, and f_y = 485 ± 15MPa at ε_y = 0.002, f_t = 630 ± 18 MPa at ε_t = 0.090 for the transverse 8-mm diameter bars, respectively.

To realize the specimens, two different concrete batches were used due to laboratory constraints, aiming in both cases at attaining a cylinder compressive strength class at 28 days of about C16/20 according to [40], that however present some differences in terms of strength and elastic properties in the two mixes. Indeed, the following experimental results (evaluated on three specimens per type and per each analyzed feature, i.e., compressive strength, tensile strength and secant elastic modulus, at 28 days) were obtained: f_{c1} = 24.1 ± 0.74 MPa, f_{ct1} = 1.15 ± 0.26 MPa, E_{c1} = 33.3 ± 4.25 GPa for the first batch; f_{c2} = 17.4 ± 2.04 MPa, f_{ct2}= 1.10 ± 0.14 MPa, E_{c2} = 19.2 ± 0.95 GPa for the second one. It is worth to recall that each trio of unconfined, confined and damaged-repaired specimens is realized with the same mix, for sake of comparison purposes. Further, three columns are labelled as damaged ones, this meaning that damaged specimens are the same unconfined columns (named as NC*)* subject to the loading protocol (described in Section 2.3) and then repaired. Hence, a direct comparison between the performance of unconfined and damaged-repaired specimens is possible.

Lastly, the specimens could be unconfined or confined, and in this latter case the FRCM jacket is realized through two-fiber layers of carbon-FRCM composite, which characteristics are reported in Section 2.2. The two-layers confinement choice was made based on a previous experimental campaign carried out by some of the authors on damaged plain concrete cylinders confined with the same fiber type obtaining strength enhancement between 10 and 20% when using this confinement configuration [39]. Overall, six samples over nine were confined.

2.2 Externally-bonded composite properties

The FRCM system was realized using balanced bidirectional carbon fiber sheets and a single-component mortar (CFRCM system). The fibers' characteristics declared by the producer were integrated by some experimental tests, needed to experimentally assess the tensile strength (f_u) and elastic modulus (E_f) values. To sum up, the properties of the carbon fiber, resulted from tests on three specimens, are: overall area weight W = 170 g/m^2, fiber elastic modulus E_f = 242 GPa, fiber tensile strength f_u = 1487 (MPa) at ultimate tensile strain ε_{fu} = 1.1%, equivalent nominal thickness t_f = 0.047 mm. The mortar is a fiber-reinforced pre-mixed one, hydrated at a water/binder ratio ranging between 0.18 and 0.22. For the repair operation, the same mortar was used. Mechanical properties (compressive and flexural strength) were experimentally evaluated according to EN 1015-11 [41], on 40x40x160 mm prisms that were casted during the repair and strengthening operations, and tested the same day of RC columns, and they are reported in Table 2 per each realized column. Values refer to average results measured at least on three samples per each analyzed property.

2.3 Experimental protocol: loading, test setup, repair and retrofit operations

The same experimental loading protocol was used for all the tested specimens, and it involves an axial loading of the columns through a displacement-control mode, during which concrete axial strains ($\varepsilon_{c,yy}$), strains into both TSR ($\varepsilon_{s,xx}$) and CFRCM fibers ($\varepsilon_{f,xx}$) were simultaneously acquired. The load was applied at a rate of 0.3mm/min, similarly than in [37], directly onto the top of the RC column, using a a 10MN capacity testing machine which mounted a 6MN capacity load cell for the continuous acquisition of the signal. In the unconfined specimens, the load was stopped after a pre-imposed

damage condition of about 30%, identified as the point in the post-peak branch corresponding to the 0.70 of the peak load (P_{max}), was reached. Such damage level is considered very significant, also compared to other works in literature aimed at verifying the effectiveness of repair systems to damaged RC specimens, where typically such value is set around 20% but might arise up to 50% [42,43].

Concerning the instrumentation used to acquire concrete axial strains, they were monitored using two types of devices, the former to describe the pre-peak and the latter to better capture the post-peak branch. In the previous case, three mechanical strain gages (mSGs), with a gauge length of 250 mm, were mounted onto the columns (cylinder) external surface at mid-height, equally spaced at 120°. In case of prismatic samples, four mSGs were used, with the same characteristics, but placed onto each sample face. Further, two linear voltage displacement transducers (LVDTs) were adopted to measure the movement of the plate mounted at each column top. Transverse strains were monitored both in the steel and in the CFRCM composite through the application of electric strain gages (eSGs). Particularly, four were applied onto the central stirrup at the column mid-height before casting operations, to evaluate TSR strains ($\varepsilon_{s,xx}$). Four were also used to evaluate fiber strains ($\varepsilon_{f,xx}$), applying directly the strain gages onto the carbon sheet, being two per each layer and located in the same position in opposite faces. Their disposition, depending on the specimen type, is shown in Figure 2. It is worth to recall that all the measures were recorded with same acquisition unit, at same frequency fixed at 5Hz.

For the damaged specimens, before the application of the FRCM jacket, a repair protocol was followed. First, an inspection of damaged regions of the tested unconfined specimens was carried out, removing the loose concrete with a hammer, and cleaning the surface with an air compressor. The appearance of the specimens at this stage is shown in Figure 3a. Then, the section of the columns was restored to the original size, using the mortar type described in Section 2.2, applying it in layer of maximum 30 mm per time as recommended by the producer, and whose characteristics are listed in Table 2. Before placing the mortar into the formwork, the concrete of the original specimens was

wetted to enhance the bond between the two materials. Lastly, after repair operation (see Figure 3b), concrete surface was superficially damped and covered with plastic wrap for one week.

Concerning instead CFRCM jacketing operation, this was carried out after 28 days from specimens manufacturing in case of strengthened ones, and after 28 days from the repair operation in case of severely-damaged samples. In both cases, the application of the composites followed the same procedure: first, specimens' surface was wetted to homogenously hydrate the support; then, a first layer of mortar was applied (Figure 4a), with an average thickness of 3 mm; the first layer of carbon sheet (instrumented with the eSGs) was then allowed to adhere to the mortar, gentle pushing into the matrix; then, the same procedure was repeated, ensuring the sheet to have an overlapping length of about 200 mm. The choice of the overlapping length used was based on a literature review on bond between FRCM systems and concrete substrates. Ombres [44] and D'Ambrisi [45] investigated bond behavior in PBO FRCM – Concrete systems reporting an effective bond length ranging between 150 mm and 200 mm; Caggegi et al. [46] reported an effective bond length related to Basalt TRM strengthening system of approximately 125 mm; Raof et al. [47] found that the effective bond length is in the range of 200-300 mm depending on the examined number of layers used. The overall thickness of the two CFRCM layers jacket was about 8 mm. It is worth to recall that the sheet was cut having an overall height of about 980 mm, thus leaving about 10 mm of empty surface per side, at the top and bottom of the specimen (Figure 4b).

3. RESULTS

3.1 Cracking pattern

All nine specimens were tested under monotonical axial compressive load while carefully monitoring axial stresses and strains, crack propagations, and strains development in the inner transverse steel reinforcement and in the outer fiber reinforcement. Collapse achievement, for the sake of comparison, is herein conventionally defined as a 20% reduction of the maximum attained load, both for confined and unconfined specimens, even though loading has been stopped at about 30% of the maximum load

drop in the unconfined specimens. Cracks opening and propagation were monitored during the loading history.

For the unconfined specimens, relevant visible cracking patterns occurred mainly in the post-peak branch, while for the confined specimens cracking displayed much earlier. For these latter, all cylinder specimens displayed a quite uniform cracking pattern in the pre-peak loading while in the post-peak loading very few new openings were observed (Figure 5). Instead, for the squared columns, existing cracks at the overlapping zone and near the edges grew at a higher rate in the post-peak branch than in the pre-peak one. Severely-damaged specimens displayed similar cracking patterns to the undamaged jacketed ones, even though more homogeneous vertical cracks were observed in the damaged squared columns compared to the undamaged ones. It is worth highlighting that confined specimens with higher TSR spacing displayed a wider cracking pattern in both damaged and undamaged conditions.

3.2 Axial stress-strain behavior

3.2.1 Undamaged bare vs. strengthened specimens

The analyzed columns were cast in two different moments resulting in two different concrete batches, having different compressive strengths but also elastic moduli as highlighted in section 2. For both batches, important enhancements of the properties were observed even though some differences in the overall axial behavior, that will be shown hereafter, may be due to such initial concrete difference. Axial behavior is discussed principally in terms of peak axial strength (f_{c0}) and corresponding axial strain (ε_{c0}), ultimate concrete stress (f_{cu}) (at 0.8 P_{max}) and corresponding ultimate axial strain (ε_{cu}) for the results of the unconfined specimens. For the confined specimens, results are presented in terms of confined axial strength (f_{cc}) and corresponding axial strain (ε_{cc}), confined ultimate stress (f_{ccu}) and corresponding ultimate axial strain (ε_{ccu}). Concrete axial stresses are computed deducing from the load recorded by the load cell the amount beared by the longitudinal bars, and then dividing it by the section area of the concrete. Recall that failure condition is conventionally considered at $0.8P_{max}$ but since the load beared by the longitudinal bars is deduced when computing concrete axial stresses, f_{cu}

(or f_{ccu}) does not correspond to 0.8 f_{c0} (or f_{cc}). Axial stress-strain curves are shown in Figure 6 comparing each trio of unconfined (continuous line), strengthened (dashed), and severely-damaged repaired (dotted) specimens.

Clear enhancements of peak strength and peak strain are observed for C20 and S33 confined specimens compared to the unconfined counterparts. Instead, an inconsistent behavior was observed for the S20_D0_C2 specimen: improvements were observed only in terms of ultimate strain, while axial strength remained almost invariant with respect to the unconfined S20_NC counterpart. Even though the same concrete batch was used for both these specimens, differences in concrete compaction and curing is believed to be the cause of this lack of improvement. Also quite low fiber strains were recorded at concrete peak strain for this specimen compared to the S33_D0_C2 and C20_D0_C2 ones. The main parameters resulting from the tests are listed in Table 3.

For undamaged specimens the best results, as expected, are obtained for the circular cross-section column with 34% increase in peak axial strength (f_{cc}) and 28% in peak strain (ε_{cc}). The squared section column S33, which also had a higher TSR spacing, showed a 27% improvement in axial strength and only 10% in peak strain. For the S20 specimen, for the reasons mentioned above, strength enhancement was limited but an important increase of 22% was observed in peak strain and nearly 30% in ultimate strain. On the other hand, S33_D0_C2 column was the only to record a slightly lower ultimate strain (92.5%) with respect to the unconfined specimen.

3.2.2 Severely-damaged repaired specimens

The main focus of the presented experimental work is to assess the effectiveness of CFRCM confinement on repairing severely-damaged RC columns, and quite promising results were observed for the three specimen types considered, as shown in Figure 6. A clear improvement in terms of axial strength with respect to the damaged conditions is observed for all specimens. As for the undamaged columns, the best performance was observed for the C20 geometry which was able to equal the attained load of the undamaged strengthened specimen, showing an increase of nearly 34% in axial strength with respect to the unconfined case. In the square-section columns, as expected, CFRCM

confinement resulted less effective than their analogue circular one. The repair was able to restore the initial strength of S20_NC (with also 3% gain) in the S20_D1_C2 specimen; instead, in the S33_D1_C2 the repair procedure was able to restore only 90% of the initial unconfined strength of S33_NC (see Table 3).

Looking at the overall stress-strain curves of undamaged specimens, in the pre-peak branch no significant differences in the axial stiffness are noted between unconfined and confined columns. As can be seen in Figure 6, differences are observed only after stress values near to f_{c0} value. On the other hand, damaged specimens show immediately a reduced axial stiffness due to their damaged condition. But while specimens with the same TSR spacing (s = 200 mm) show similar elastic modulus reduction regardless of the cross-section shape, specimen S33_D1_C2 displays a more pronounced difference between undamaged and damaged secant modulus since relatively small stress values (nearly to 6 MPa). As damage level is relatively similar in all specimens, it is believed that TSR high spacing is the main factor to which this difference is due.

When considering undamaged RC columns confined with CFRCM, the confinement system effectiveness seems similar in terms of peak strength (f_{c0}) and strain (ε_{cc}) development, with gains varying in the order of 10-34%, as discussed in section 3.2.1. This is not the case when dealing with severely damaged columns. The CFRCM system for the damaged columns with the lowest TSR spacing (i.e., C20 and S20) was able to restore at least the initial strength of the unconfined specimens. However, in none of the above, it was possible to restore the peak strain of the unconfined specimens, reaching only 65% and 78% of ε_{c0}, respectively. The confined damaged specimen with the highest TSR spacing (i.e., S33_D1_C2) could not restore the initial unconfined strength, probably due to its lower axial stiffness previously discussed, and reached its peak strength at an axial strain 10% higher than its unconfined case.

However, when assessing the effectiveness of CFRCM confinement on repairing severely-damaged RC elements, the authors believe that it is not entirely appropriate to refer to the initial resistance of the undamaged condition only. Indeed, since repairing is done on an already damaged element, it

results more significant to evaluate the effectiveness of the intervention referring to the residual axial strength of the columns at the end of the previous loading history. In Table 3, the residual axial strength values for each unconfined specimens are reported under the parameter $f_{u,D,}$ and the effectiveness of the repair operation is evaluated through the $f_{cc}/f_{u,D}$ ratio. It can be seen that through the CFRCM confinement, all repaired specimens have significantly enhanced their residual axial capacity. The circular-shaped section is still the most effective with an increment of the repaired axial capacity with respect to the residual capacity of the severely-damaged element of nearly 118%. The squared-shape sections result less effective than the circular one, but were still able to enhance their damaged residual capacity by 73% for the S20_D1_C2 and by 41% for the S33_D1_C2 specimen. It is important to highlight how, apart from the influence of the cross-section shape in the effectiveness of the CFRCM confinement, the spacing of internal TSR is of fundamental importance in the overall confinement effectiveness.

3.2 Fiber and TSR strain development

Strain development was monitored in all specimens in the central stirrup using four eSGs and in the FRCM layers for the externally confined specimens using two eSGs per layer applied on the opposite faces of the columns, as better detailed in Section 2.3. Results are shown in Figures 7-8 for unconfined (continuous line), strengthened (dashed), and severely-damaged repaired (dotted) specimens. Fully opaque lines represent the mean strain values while transparent lines show the trend of single eSGs.

3.2.1 TSR strains

Figure 7 shows in detail TSR strains evolution in (a) C20, (b) S20 and (c) S33 columns, in all the three analyzed conditions. The circular-section C20 geometry recorded the lowest strains compared to the square-section columns for all three considered conditions. Particularly low strain values were recorded in the unconfined and strengthened specimens (i.e., C20_NC and C20_D0_C2). This may be due to damage concentration on the upper part of the column which may have solicited more those stirrups in the highest positions (see Figure 5), which unfortunately were not being monitored.

For the undamaged columns, strains in the TSR grow at the same rate in both confined and unconfined elements. A slight difference is noted only in the S33 undamaged specimens, where at axial stress of about 9 MPa the TSR strain rate becomes slightly higher for the unconfined specimen. Generally, TSR strains development started earlier for damaged specimens, which also developed higher values than the undamaged ones. It is interesting to notice the difference in the strain rate development between circular- and square-section columns. Strain rates in the pre-peak branch of the curve result much higher for the squared shape sections, while the circular one shows strain rates closer to the undamaged conditions, which grow faster at axial stress levels near to the unconfined strength (f_{c0}). For damaged square-section columns (i.e., S20_D1_C2 and S33_D1_C2) TSR strains grow at higher rates after stress levels of about 0.25-0.30 f_{cc}.

Table 4 reports mean strain values for TSR and FRCM at peak and ultimate stresses. Comparing TSR strains at peak load among undamaged specimens, very similar values are recorded. $\varepsilon_{s,xx}$ of the C20_NC is a little less than 0.1‰, while also the confined one C20_D0_C2 recorded strains slightly above 0.1‰. The squared S20 undamaged specimens recorded also similar TSR strains of nearly 0.18‰ and 0.20‰, respectively for the unconfined and confined situations. On the other hand, the S33 specimens recorded lower TSR strains in the confined condition (0.33‰) with respect to the unconfined one (0.68‰). It seems that higher TSR strain values at peak stress are recorded in specimens with less effective confinement systems, both in terms of section-shape and reinforcement spacing. This order is maintained also for TSR strains at ultimate stress with higher strains recorded in the S33 column followed by the S20 and C20 ones.

Discussing the strain evolutions on damaged columns (i.e., those specimens labelled with “D1”), the results show TSR strains at peak load that are almost five times higher than the ones recorded in the confined but undamaged cases (i.e., D0). C20_D1_C2 specimen recorded a mean TSR strain of 0.5‰ (instead of 0.1‰ recorded in C20_D0_C2), S20_D1_C2 TSR strain was about 1.1‰ (instead of 0.2‰ in S20_D0_C2) and the same trend was observed in the S33 geometry, where the damaged case S33_D1_C2 recorded 1.58‰ (instead of 0.33‰ in S33_D0_C2).

3.2.2 Fiber and TSR strains in the confined columns

Measuring local strains in the FRCM jacketing experimentally is a harsh task and not always repays with the expected results. The possibility that cracks open at eSG location or that eSGs are located between two cracks, being so affected by tension stiffening phenomena, may result in quite variable strain records. To guarantee reliable results, high numbers of eSGs distributed through the reinforcement layers must be applied, but this cost efforts and especially can result uneconomic. However, in this experimental campaign good results were obtained also for the monitored fiber strains. Few eSGs with discordant records were discarded from the final results. Figure 8 compares TSR and fiber strains in the damaged specimens in (a) C20_D1_C2, (b) S20_D1_C2 and (c) S33_D1_C2 specimens, while fiber strain values at peak and ultimate stress are listed in Table 5, in its last two columns. In the pre-peak condition, C20_D1_C2 and S33_D1_C2 develop TSR and fiber strains at almost the same rate. In the S20_D1_C2 specimen, significant fiber strains were recorded only after stress levels of nearly 0.6 f_{cc}, while TSR strains start growing almost immediately. Different trends are observed in the post-peak branch for circular- and square-section specimens. In the C20_D1_C2 specimen, after peak stress, fiber strains grow at higher rate than TSR strains. This means that the FRCM system plays a bigger role than the TSR in the axial ductility of the confined RC element. In both square-section columns, TSR and fiber strains follow almost the same trend in the post-peak behavior, with TSR final strains being slightly higher than the fiber ones in the S20 case and almost the same strains in the S33 geometries. Peak strains recorded in TSR and fibers were quite similar in all specimens, with some differences only in the S33 specimen. The circular-section column C20_D1_C2 recorded lower peak strain values (0.4‰ for fibers and 0.5‰ for TSR) compared to those in squared columns, which were more than the double. On the other hand, fiber strains at ultimate stress were higher in the circular shaped section, which explains, along with the more effective section shape, the slightly more ductile behavior this specimen showed (Figure 6).

It is also worth mentioning that in C20 and S20 specimens no significant differences were noted in the strains recorded in the different layers of the CFRCM system while in the S33 specimens fiber exploitation resulted higher in the first CFRCM layer.

4. DISCUSSION

4.1 Cross-section geometry effect

Cross-section shape is known to be an important factor when dealing with confinement systems and its influence remains important even when repairing damaged RC elements. Figure 9 compares axial stress-strain curves relative to the initial strength of unconfined specimens f_{c0} (a) and to the remaining capacity of the damaged specimens $f_{u,D}$ (b). Cross-section shape effect is evident when comparing C20 and S20 geometries, characterized by the same TSR and fiber rate. C20_D1_C2 specimen results nearly 30% more effective than the squared-shape column in terms of both $f_{cc}/f_{u,D}$ and f_{cc}/f_{c0} rates. On the other hand, TSR influence on the overall behavior of the repaired elements is well highlighted comparing specimens S20 and S33, that differ only by the stirrups spacing (i.e. 200 and 330 mm). The effect of stirrup spacing is clearer in Figure 9.b, which considers the repaired strength f_{cc} with respect to the residual strength $f_{u,D}$ of the damaged specimens. The repaired S20 specimen resulted 25% more effective than the same specimen with 330 mm stirrup spacing (S33). Comparing f_{cc}/f_{c0} rates only, the S20 specimens would result only 14% more effective than the S33. These results indicate that cross-section shape and fiber-TSR interaction can significantly influence the overall behavior of damaged elements repaired through CFRCM confinement.

Cross-sectional shape influences also the development of lateral strains in TSR and fiber reinforcement. Figure 10 compares lateral TSR strains in unconfined (a) and in strengthened specimens (b). Similar trends can be seen between NC and D0_C2 series: there, square-shaped columns record higher lateral stirrup strains in both confined and unconfined cases. Also, in the post-peak branch, TSR strains tend to decrease faster in the circular shape with respect to the squared ones. Figure 11 shows TSR strains (a) and fiber strains (b) for the damaged specimens, showing the same

trend described before about the influence of cross-section geometry on the development of ε_{xx} in the central stirrup.

4.2 Lateral pressure and Fiber-TSR interaction

Generally, confinement effectiveness is considered in concrete confinement models [5, 48-51], whether they are dealing with internally confined (TSR) or externally (FRP, FRCM) confined concrete, through effectiveness coefficients (k_s & k_f). For continuous FRCM jacketing the horizontal efficiency coefficient $k_{f,h}$ depends on the corner radius r and on the cross-section dimensions b and h for rectangular shape, while for circular cross-section this coefficient is assumed to be unitary.

$$k_{f,h} = 1 - \frac{(b-2r)^2+(h-2r)^2}{3bh} \quad (1)$$

Other effectiveness coefficients can be considered to account for fiber orientation with respect to the member axial axis ($k_{f,a}$) or for vertical efficiency in partially wrapped systems ($k_{f,v}$), which are assumed unitary for the analyzed configurations used in this experimental campaign.

For internal confinement by TSR, the geometric effectiveness coefficient does not depend on corner radius but only on the layout and spacing of TSR and can be computed following the Mander et al. approach [48] for circular cross-sections:

$$k_s = \frac{A_e}{(1-\rho_{cc})A_c} = \frac{\left(1-{s'}/{2d_s}\right)^2}{1-\rho_{cc}} \quad (2)$$

and for rectangular ones:

$$k_s = \frac{\left[(1-\sum_{i=1}^{n}\frac{(w_i')^2}{6b_cd_c})(1-\frac{s'}{2b_c})(1-\frac{s'}{2d_c})\right]}{(1-\rho_{cc})} \quad (3)$$

where A_e is the effectively confined concrete area; A_c is the concrete core area; ρ_{cc} is the longitudinal reinforcement ratio to the core area; s' is the clear vertical spacing between consecutive stirrups; d_s is the hoop diameter for circular cross-sections; w_i' is the i-th clear distance between adjacent longitudinal bars; b_c and d_c are the concrete core dimensions taken between stirrups centerlines.

Once the effectiveness coefficients are known, the lateral confining pressure can be computed for both internal TSR:

$$f_{ls} = \frac{1}{2} k_s \rho_{st} \sigma_{st} \quad (4)$$

and external FRCM system:

$$f_{lf} = \frac{1}{2} k_f \rho_f \sigma_f \quad (5)$$

where ρ_{st} and ρ_f are the volumetric ratio of TSR and FRCM and σ_{st} and σ_f are stresses in stirrup and fibers.

For rectangular cross-sections, the confining pressure should be computed separately in the two main directions ($f_{ls,x}$ and $f_{ls,y}$), since for non-symmetrical sections lateral pressure can be different. Mander et al. [48] sets σ_{st} equal to the yielding stress of the reinforcement.

Pellegrino & Modena [5] studied the interaction between internal TSR and external FRP confinement proposing an additive model to compute the overall confining pressure offered by both systems. However, such interaction is not yet studied for FRCM confining systems and existing models generally neglect TSR contribution. The issue is even less clear when it comes to repairing and not just strengthening of existing structures. To investigate this phenomenon, strain data on both fibers and TSR were collected experimentally through electrical strain gages. The experimental data gathered in this campaign suggest that, at least for damaged elements, TSR contribution and fiber-TSR interaction are important factors in the behavior of damaged RC elements repaired through FRCM confinement, since they grow at similar rates both in the pre- and post-peak branches of stress-strain curves.

Fiber and TSR mean strain values for peak and ultimate load are reported in Table 4. Based on these strain values and on the effectiveness coefficients computed as shown in the above equations, confining pressure exerted by TSR and FRCM at peak and ultimate (80%) load was computed and reported in Table 5. Also, the total confining pressure $f_{l,tot}$, computed as the sum of TSR and fiber pressure, is given for peak and ultimate load.

It can be noted that the confining pressure exerted by TSR (f_{ls}) at peak load is almost the same for specimens with the same stirrup spacing regardless of their cross-section. TSR confining pressure is

significantly lower for the S33 geometries than in all other cases. On the other hand, FRCM provides continuous confinement to the columns and is more influenced by cross-section shape than TSR, thus varying more between prismatic and cylinder columns. For damaged and repaired columns, confining pressure at peak load exerted by fibers results similar for S20 and S33 specimens, while the circular one (C20) displays slightly smaller lateral pressure. This value becomes much bigger in the post-peak branch, exceeding largely those values recorded by the specimens with the square cross-section.

In the S33 specimens, FRCM contribution to the overall confinement results significantly higher than the TSR effect. Instead, for 200 mm stirrup spacing, fiber and TSR contribution to the overall confining pressure at peak load becomes similar, even though, a higher TSR effect is seen in the circular section. At the ultimate load, FRCM confining pressure results more than double the TSR pressure in the circular shaped specimens while in the squared one the two pressures result quite comparable. Considering the total confining pressure as a simple addition of the TSR and fiber contributions, the highest value (0.169 MPa) at peak load is recorded in the S20 specimens while for ultimate load in the C20 one (0.688 MPa). In the undamaged specimens, fiber confining pressure resulted in smaller and more dispersive values.

The results in terms of lateral confinement pressure highlight how neglecting the contribution of transverse reinforcement, as existing models on FRCM confinement of concrete currently do, is an assumption that does not reflect the actual behavior, at least for elements with not too large stirrups spacing. In addition, recalling the results in terms of strength enhancement after repair, where the circular-shaped column performed undoubtedly better than the squared-section ones, results show also that a simple additive contribution of the two reinforcements does not well describe the overall behavior and particularly the interaction of the two reinforcements under the axial loading.

5. CONCLUSIONS

The experimental work presented in this paper aimed to study the effectiveness of FRCM systems to adequately repair RC columns through confinement. Two different cross-section shapes (circular and

squared) and two TSR spacing (200 and 330 mm) were considered in full-scale specimens. Results of repaired specimens were then compared to the results of unconfined undamaged specimens and FRCM confined undamaged RC specimens. Hoop strains were monitored in both TSR and fibers to evaluate the effective confining pressure and possible interaction between internal and external confining systems. Based on the experimental results previously discussed, the following conclusions can be drawn:

- repair through CFRCM confinement was able to enhance concrete strength in all considered specimens. Compared to the residual axial capacity of the damaged specimens, the repair protocol was able to enhance concrete strength by a factor of 2.18 in the circular-shaped C20_D1 specimen, 1.75 in the squared-shape S20_D1 and 1.40 in the squared-shape S33_D1 specimen;
- cross-section shape and TSR spacing have an important effect in the overall repair effectiveness. The circular-shaped specimen C20_D1_C2 was able to match the resistance of the undamaged FRCM confined C20_D0_C2 specimen while the squared S20_D1_C2 equaled the undamaged C20_NC resistance. The squared specimen with higher TSR spacing was able to reach only 90% of the S33_NC strength;
- peak and ultimate axial strain did not improve much in all repaired specimens and resulted in lower values with respect to the NC series, apart specimen S33_D1_C2 which stress-strain curve resulted in a slightly different trend with respect to the other two;
- damaged specimens developed lateral strains in TSR and fibers at higher rates than undamaged ones. Higher strain values were recorded in specimens with less effective confining systems due to both section-shape and TSR ratio. Similar trends were noted for TSR and fiber strains in all specimens;
- estimated confining pressure exerted by TSR and FRCM confinement highlights the importance of TSR spacing and the results seems to suggest that a simple additive model of the two contributions (fiber & TSR) might not be the best solution to describe the interaction between the internal and external confining systems.

It is important to emphasize that further research on this issue is needed given the lack of existing studies that experimentally investigate FRCM-TSR interaction in concrete confinement and the limited number of specimens, due to their real scale dimensions, investigated in the present one.

REFERENCES

[1] McGarry, F. J. (1970). Building design with fibre reinforced materials. *Proceedings of the Royal Society of London. A. Mathematical and Physical Sciences*, *319*(1536), 59-68.

[2] Fardis, M. N., & Khalili, H. H. (1982). FRP-encased concrete as a structural material. *Magazine of Concrete Research*, *34*(121), 191-202.

[3] Campione, G., Colajanni, P., La Mendola, L., & Spinella, N. (2007). Ductility of reinforced concrete members externally wrapped with fiber-reinforced polymer sheets. *Journal of Composites for Construction*, 11(3), 279-290.

[4] Mirmiran, A., Shahawy, M., Samaan, M., Echary, H. E., Mastrapa, J. C., & Pico, O. (1998). Effect of column parameters on FRP-confined concrete. *Journal of Composites for Construction*, 2(4), 175-185.

[5] Pellegrino, C., & Modena, C. (2010). Analytical model for FRP confinement of concrete columns with and without internal steel reinforcement. *Journal of Composites for Construction*, 14(6), 693-705.

[6] Realfonzo, R., & Napoli, A. (2011). Concrete confined by FRP systems: confinement efficiency and design strength models. *Composites Part B: Engineering*, 42(4), 736-755.

[7] Saadatmanesh, H., Ehsani, M. R., & Jin, L. (1997). Repair of earthquake-damaged RC columns with FRP wraps. *ACI Structural Journal*, *94*, 206-215.

[8] Li, G., Hedlund, S., Pang, S. S., Alaywan, W., Eggers, J., & Abadie, C. (2003). Repair of damaged RC columns using fast curing FRP composites. *Composites Part B: Engineering*, *34*(3), 261-271.

[9] Faleschini, F., Gonzalez-Libreros, J., Zanini, M. A., Hofer, L., Sneed, L., & Pellegrino, C. (2019). Repair of severely-damaged RC exterior beam-column joints with FRP and FRCM composites. *Composite Structures*, *207*, 352-363.

[10] Eid, R., & Paultre, P. (2008). Analytical model for FRP-confined circular reinforced concrete columns. *Journal of Composites for Construction*, 12(5), 541-552.

[11] Teng, J. G., Lin, G., & Yu, T. (2015). Analysis-oriented stress-strain model for concrete under combined FRP-steel confinement. *Journal of Composites for Construction*, 19(5), 04014084.

[12] Lin, G., Yu, T., & Teng, J. G. (2016). Design-oriented stress–strain model for concrete under combined FRP-steel confinement. *Journal of Composites for Construction*, 20(4), 04015084.

[13] Al-Rahmani, A., & Rasheed, H. (2016). Combined Transverse Steel-External FRP Confinement Model for Rectangular Reinforced Concrete Columns. *Fibers*, 4(1), 8.

[14] Kaeseberg, S., Messerer, D., & Holschemacher, K. (2020). Experimental Study on Concrete under Combined FRP–Steel Confinement. *Materials*, 13(20), 4467.

[15] Bournas, G. Cerniauskas Z. Tetta DA, & Bisby L.A. (2020). Concrete confinement with TRM versus FRP jackets at elevated temperatures. *Materials and Structures 53*: 58.

[16] Lionetto F,, Aiello, M.A., & Maffezzoli, A. (2018). Reversible FRP-confinement of heritage masonry columns. In: *9th International Conference on Fibre-Reinforced Polymer (FRP) Composites in Civil Engineering* (CICE 2018), 2018, Paris 17–19 July 2018.

[17] Zhao, J., & Vokkarane, V.M. (2017). Reverse manycast data retrieval in Elastic Optical Networks, In: *2017 International Conference on Computing, Networking and Communications (ICNC)*, Santa Clara, CA, 2017, pp. 402-407, doi: 10.1109/ICCNC.2017.7876162.

[18] Bencardino, F., Carloni, C., Condello, A., Focacci, F., Napoli, A., & Realfonzo, R. (2018). Flexural behaviour of RC members strengthened with FRCM: State-of-the-art and predictive formulas. *Composites Part B: Engineering*, *148*, 132-148.

[19] Sneed, L. H., Verre, S., Carloni, C., & Ombres, L. (2016). Flexural behavior of RC beams strengthened with steel-FRCM composite. *Engineering Structures*, *127*, 686-699.

[20] Raoof, S. M., Koutas, L. N., & Bournas, D. A. (2017). Textile-reinforced mortar (TRM) versus fibre-reinforced polymers (FRP) in flexural strengthening of RC beams. *Construction and Building Materials*, *151*, 279-291.

[21] El-Sherif, H., Wakjira, T. G., & Ebead, U. (2020). Flexural strengthening of reinforced concrete beams using hybrid near-surface embedded/externally bonded fabric-reinforced cementitious matrix. *Construction and Building Materials*, 238, 117748.

[22] Gonzalez-Libreros, J. H., Sneed, L. H., D'Antino, T., & Pellegrino, C. (2017). Behavior of RC beams strengthened in shear with FRP and FRCM composites. *Engineering Structures*, *150*, 830-842.

[23] Wakjira, T. G., & Ebead, U. (2019). A shear design model for RC beams strengthened with fabric reinforced cementitious matrix. *Engineering Structures*, *200*, 109698.

[24] Triantafillou, T. C., & Papanicolaou, C. G. (2006). Shear strengthening of reinforced concrete members with textile reinforced mortar (TRM) jackets. *Materials and Structures*, 39(1), 93-103.

[25] Mofidi, A., Cheng, L., Chaallal, O., & Shao, Y. (2018). Shear Strengthening of RC Beams with NSM FRP—Influencing Parameters and A Theoretical Model. *ACI Special Publication*, 327, 31-1.

[26] Fossetti, M., Alotta, G., Basone, F., & Macaluso, G. (2017). Simplified analytical models for compressed concrete columns confined by FRP and FRCM system. *Materials and Structures*, *50*(6), 240.

[27] Murgo, F. S., & Mazzotti, C. (2019). Masonry columns strengthened with FRCM system: Numerical and experimental evaluation. *Construction and Building Materials*, 202, 208-222.

[28] Incerti, A., Vasiliu, A., Ferracuti, B., & Mazzotti, C. (2015). Uni-Axial compressive tests on masonry columns confined by FRP and FRCM. In: *Proc. of the 12th International Symposium on Fiber Reinforced Polymers for Reinforced Concrete Structures & The 5th Asia-Pacific Conference on Fiber Reinforced Polymers in Structures, Joint Conference*, Nanjing, China, 14–16 December 2015.

[29] Colajanni, P., Fossetti, M., & Macaluso, G. (2014). Effects of confinement level, cross-section shape and corner radius on the cyclic behavior of CFRCM confined concrete columns. *Construction and Building Materials*, *55*, 379-389.

[30] Ombres, L. (2007). Confinement effectiveness in concrete strengthened with fiber reinforced cement based composite jackets. In: *Proc., FRPRCS-8, 8th Int. Symp. on Fiber Reinforced Polymer Reinforcement for Concrete Structures*, T. C. Triantafillou, ed., Univ. of Patras, Patras, Greece.

[31] Ombres, L. (2014). Concrete confinement with a cement based high strength composite material. *Composite Structures*, *109*, 294-304.

[32] Ombres, L., & Mazzuca, S. (2017). Confined concrete elements with cement-based composites: confinement effectiveness and prediction models. *Journal of Composites for Construction*, 21(3), 04016103.

[33] Triantafillou, T. C., Papanicolaou, C. G., Zissimopoulos, P., & Laourdekis, T. (2006). Concrete confinement with textile-reinforced mortar jackets. *ACI Materials Journal*, 103(1), 28.

[34] Gonzalez-Libreros, J., Zanini, M. A., Faleschini, F., & Pellegrino, C. (2019). Confinement of low-strength concrete with fiber reinforced cementitious matrix (FRCM) composites. *Composites Part B: Engineering*, 177, 107407.

[35] Bournas, D. A., Lontou, P. V., Papanicolaou, C. G., & Triantafillou, T. C. (2007). Textile-reinforced mortar versus fiber-reinforced polymer confinement in reinforced concrete columns. *ACI Structural Journal*, 104(6), 740.

[36] Faleschini, F., Zanini, M. A., Hofer, L., & Pellegrino, C. (2020). Experimental behavior of reinforced concrete columns confined with carbon-FRCM composites. *Construction and Building Materials*, *243*, 118296.

[37] Faleschini, F., Zanini, M. A., Hofer, L., Toska, K., De Domenico, D., & Pellegrino, C. (2020). Confinement of reinforced concrete columns with glass fiber reinforced cementitious matrix jackets. *Engineering Structures*, *218*, 110847.

[38] Peled, A. (2007). Confinement of damaged and nondamaged structural concrete with FRP and TRC sleeves. *Journal of Composites for Construction*, *11*(5), 514-522.

[39] Gonzalez-Libreros, J., Sabau, C., Sneed, L. H., Sas, G., & Pellegrino, C. (2017, September). Effect of confinement with FRCM composites on damaged concrete cylinders. In *International Conference on Strain-Hardening Cement-Based Composites* (pp. 770-777). Springer, Dordrecht.

[40] EN 206 (2013). Concrete. Specification, performance, production and conformity. European Committee for standardization, Brussels, Belgium.

[41] EN 1015-11 (2019). Methods of test for mortar for masonry. Determination of flexural and compressive strength of hardened mortar. European Committee for standardization, Brussels, Belgium.

[42] Chellapandian, M., Prakash, S. S., & Sharma, A. (2019). Axial compression–bending interaction behavior of severely damaged RC columns rapid repaired and strengthened using hybrid FRP composites. *Construction and Building Materials*, 195, 390-404.

[43] He, R., Sneed, L. H., & Belarbi, A. (2013). Rapid repair of severely damaged RC columns with different damage conditions: An experimental study. *International Journal of Concrete Structures and Materials*, 7(1), 35-50.

[44] Ombres, L. (2015). Analysis of the bond between fabric reinforced cementitious mortar (FRCM) strengthening systems and concrete. *Composites Part B*: Engineering, 69, 418-426.

[45] D'Ambrisi, A., Feo, L., & Focacci, F. (2012). Bond-slip relations for PBO-FRCM materials externally bonded to concrete. *Composites Part B*: Engineering, 43(8), 2938-2949.

[46] Caggegi, C., Sciuto, D., & Cuomo, M. (2018). Experimental study on effective bond length of basalt textile reinforced mortar strengthening system: Contributions of digital image correlation. *Measurement*, 129, 119-127.

[47] Raoof, S. M., Koutas, L. N., & Bournas, D. A. (2016). Bond between textile-reinforced mortar (TRM) and concrete substrates: Experimental investigation. *Composites Part B*: Engineering, 98, 350-361.

[48] Mander, J. B., Priestley, M. J., & Park, R. (1988). Theoretical stress-strain model for confined concrete. *Journal of Structural Engineering*, 114(8), 1804-1826.

[49] Spoelstra, M. R., & Monti, G. (1999). FRP-confined concrete model. *Journal of composites for construction*, 3(3), 143-150.

[50] Bisby, L. A., Dent, A. J., & Green, M. F. (2005). Comparison of confinement models for FRP wrapped concrete. *ACI Structural Journal*, 62-72.

[51] Lam, L., & Teng, J. G. (2003). Design-oriented stress–strain model for FRP-confined concrete. *Construction and Building Materials*, 17(6-7), 471-489.

TABLES

Table 1. Specimens characteristics.

Specimen ID	Geometry			Steel Reinforcement *B450C*		Concrete		FRCM Confinement	
	Section geometry	Specimen dimensions (mm)	Corner radius	A_{sl} (mm^2)	A_{sw} (mm^2/m)	Concrete batch f_{cm} (MPa)	Concrete Damage	Presence	Number of layers
C20_NC	cylinder	d = 300; h = 1000	-	615	502	17.4	-	no	-
S20_NC	square	l = 300; h = 1000	20	615	502	17.4	-	no	-
S33_NC	square	l = 300; h = 1000	20	615	301	24.1	-	no	-
C20_D0_C2	cylinder	d = 300; h = 1000	-	615	502	17.4	-	yes	2
S20_D0_C2	square	l = 300; h = 1000	20	615	502	17.4	-	yes	2
S33_D0_C2	square	l = 300; h = 1000	20	615	301	24.1	-	yes	2
C20_D1_C2	cylinder	d = 300; h = 1000	-	615	502	17.4	yes, 70%	yes	2
S20_D1_C2	square	l = 300; h = 1000	20	615	502	17.4	yes, 70%	yes	2
S33_D1_C2	square	l = 300; h = 1000	20	615	301	24.1	yes, 70%	yes	2

Table 2. FRCM and repair mortar properties

Specimen ID	FRCM mortar			Repair mortar		
	ρ (kg/m^3)	f_{cm} (MPa)	$f_{cm,f}$ (MPa)	ρ (kg/m^3)	f_{cm} (MPa)	$f_{cm,f}$ (MPa)
C20_D0_C2	1880 ± 22	30.88 ± 0.78	5.08 ± 0.27	-	-	-
S20_D0_C2	1877 ± 12	32.14 ± 0.62	6.12 ± 0.94	-	-	-
S33_D0_C2	1947 ± 11	33.56 ± 1.81	5.50 ± 1.06	-	-	-
C20_D1_C2	2046 ± 34	21.06 ± 1.39	4.96 ± 0.26	2153 ± 5	22.81 ± 3.76	5.93 ± 0.27
S20_D1_C2	2114 ± 48	23.22 ± 1.62	4.77 ± 0.37	2143 ± 40	21.58 ± 1.59	5.08 ± 0.36
S33_D1_C2	2047 ± 19	20.71 ± 1.16	4.92 ± 0.43	2091 ± 78	28.20 ± 2.30	5.41 ± 0.90

Table 3. Specimens test results

Specimen ID	$f_{c0(cc)}$ [MPa]	$f_{cu(ccu)}$ [MPa]	$f_{u,D}$ [MPa]	$e_{c0(cc)}$ [-]	$e_{cu(ccu)}$ [-]	f_{cc}/f_{c0} [-]	f_{ccu}/f_{cu} [-]	e_{cc}/e_{c0} [-]	e_{ccu}/e_{cu} [-]	$f_{cc}/f_{u,D}$ [-]
C20_NC	13.15	9.62	8.08	0.0029	0.0065	-	-	-	-	-
S20_NC	14.20	10.58	8.38	0.0018	0.0054	-	-	-	-	-
S33_NC	16.58	12.52	10.68	0.0020	0.0040	-	-	-	-	-
C20_D0_C2	17.63	13.21	-	0.0037	0.0072	1.34	1.376	1.276	1.107	-
S20_D0_C2	14.34	10.71	-	0.0022	0.0070	1.01	1.012	1.222	1.296	-
S33_D0_C2	21.09	16.43	-	0.0022	0.0037	1.27	1.312	1.100	0.925	-
C20_D1_C2	17.62	13.02	-	0.0019	0.0050	1.34	1.353	0.655	0.770	2.180
S20_D1_C2	14.67	10.20	-	0.0014	0.0040	1.03	0.964	0.777	0.741	1.750
S33_D1_C2	14.98	12.05	-	0.0022	0.0046	0.90	0.962	1.100	1.150	1.402

Table 4. Mean TSR and fiber hoop strains at peak and ultimate stress

Specimen ID	$\varepsilon_{s,xx\ (peak)}$ [‰]	$\varepsilon_{s,xx\ (ultimate)}$ [‰]	$\varepsilon_{f,xx\ (peak)}$ [‰]	$\varepsilon_{f,xx\ (ultimate)}$ [‰]
C20_NC	0.0877	0.3585	-	-
S20_NC	0.1762	1.1826	-	-
S33_NC	0.6764	2.3388	-	-
C20_D0_C2	0.1073	0.1646	0.2172	0.2805
S20_D0_C2	0.1971	1.3880	0.1264	0.4285
S33_D0_C2	0.3258	1.7170	0.2520	0.6281
C20_D1_C2	0.5070	1.2074	0.4017	3.2342
S20_D1_C2	1.1069	2.3229	1.0629	2.0963
S33_D1_C2	1.5811	2.3113	1.1363	2.3398

Table 5. Confining pressure exerted from CFRCM and TSR

					peak			ultimate		
Specimen ID	ρ_s	k_s	ρ_f	k_f	f_{ls} [MPa]	f_{lf} [MPa]	$f_{l,tot}$ [MPa]	f_{ls} [MPa]	f_{lf} [MPa]	$f_{l,tot}$ [MPa]
C20_NC	0.00387	0.403	-	-	0.014	-	0.014	0.059	-	0.059
S20_NC	0.00387	0.197	-	-	0.014	-	0.014	0.095	-	0.095
S33_NC	0.00234	0.067	-	-	0.009	-	0.009	0.038	-	0.038
C20_D0_C2	0.00387	0.403	0.00125	1.000	0.018	0.033	0.050	0.027	0.043	0.069
S20_D0_C2	0.00387	0.197	0.00125	0.499	0.016	0.010	0.025	0.111	0.032	0.144
S33_D0_C2	0.00234	0.067	0.00125	0.499	0.005	0.019	0.024	0.028	0.048	0.076
C20_D1_C2	0.00387	0.403	0.00125	1.000	0.083	0.061	0.144	0.197	0.490	0.688
S20_D1_C2	0.00387	0.197	0.00125	0.499	0.089	0.080	0.169	0.186	0.159	0.345
S33_D1_C2	0.00234	0.067	0.00125	0.499	0.026	0.086	0.112	0.038	0.177	0.215

FIGURES

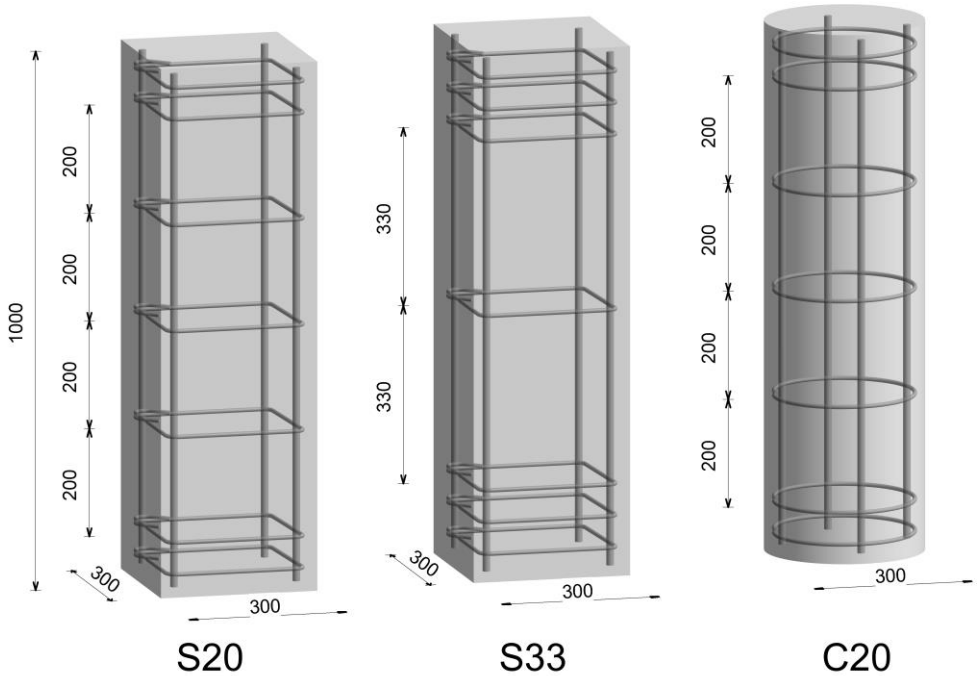

Figure 1. Reinforcement details.

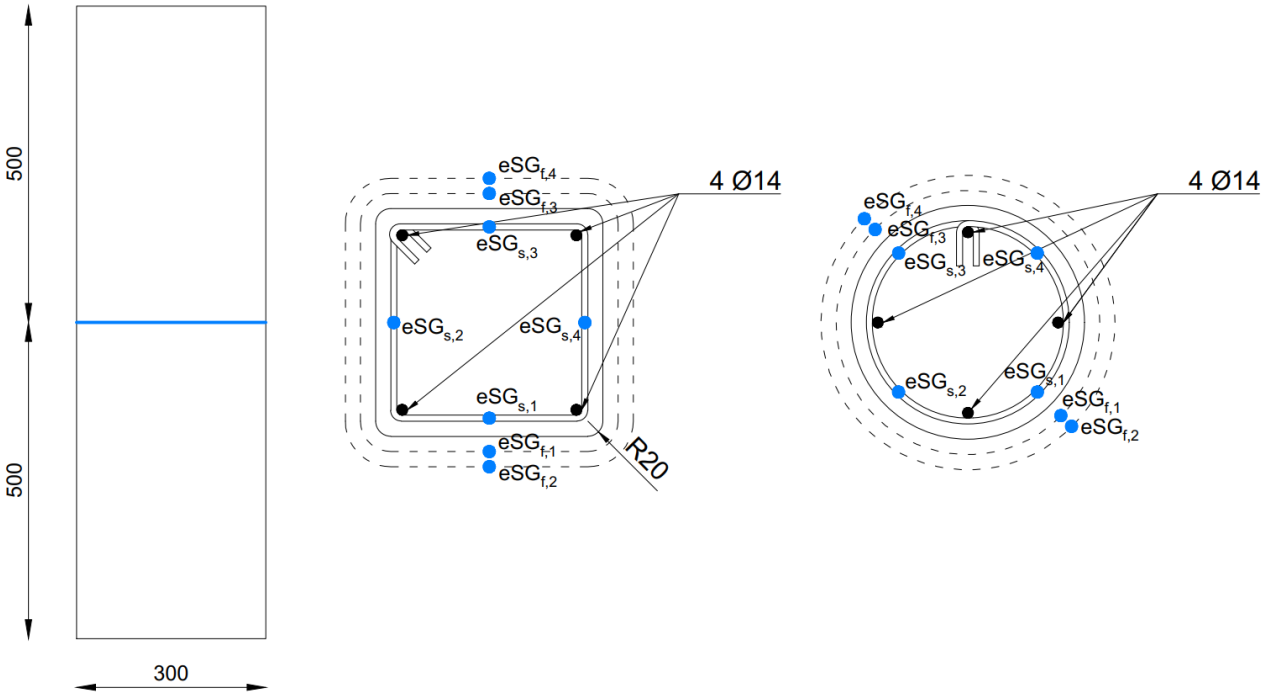

Figure 2. Disposition of eSGs to evaluate stirrup and fibers strains.

Figure 3. S33_NC specimen after failure (a); S33_NC specimen after repair operation (b).

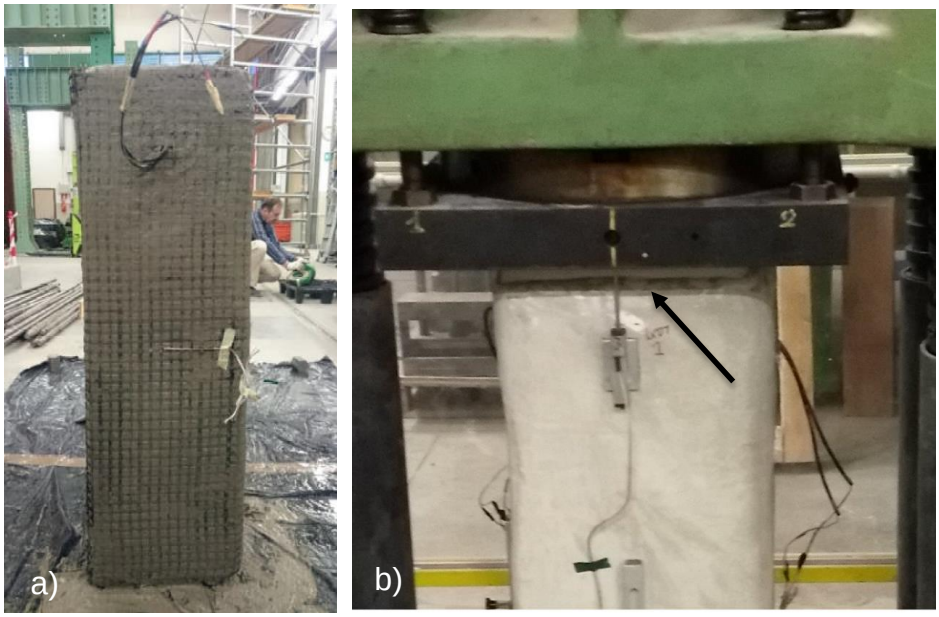

Figure 4. Application of the first FRCM layer onto the S33_D1_C2 specimen (a); detail of the top of S33_D1_C2 specimen prior to the test (b).

Figure 5. C20_NC, C20_D0_C2 and C20_D1_C2 at the end of the loading history

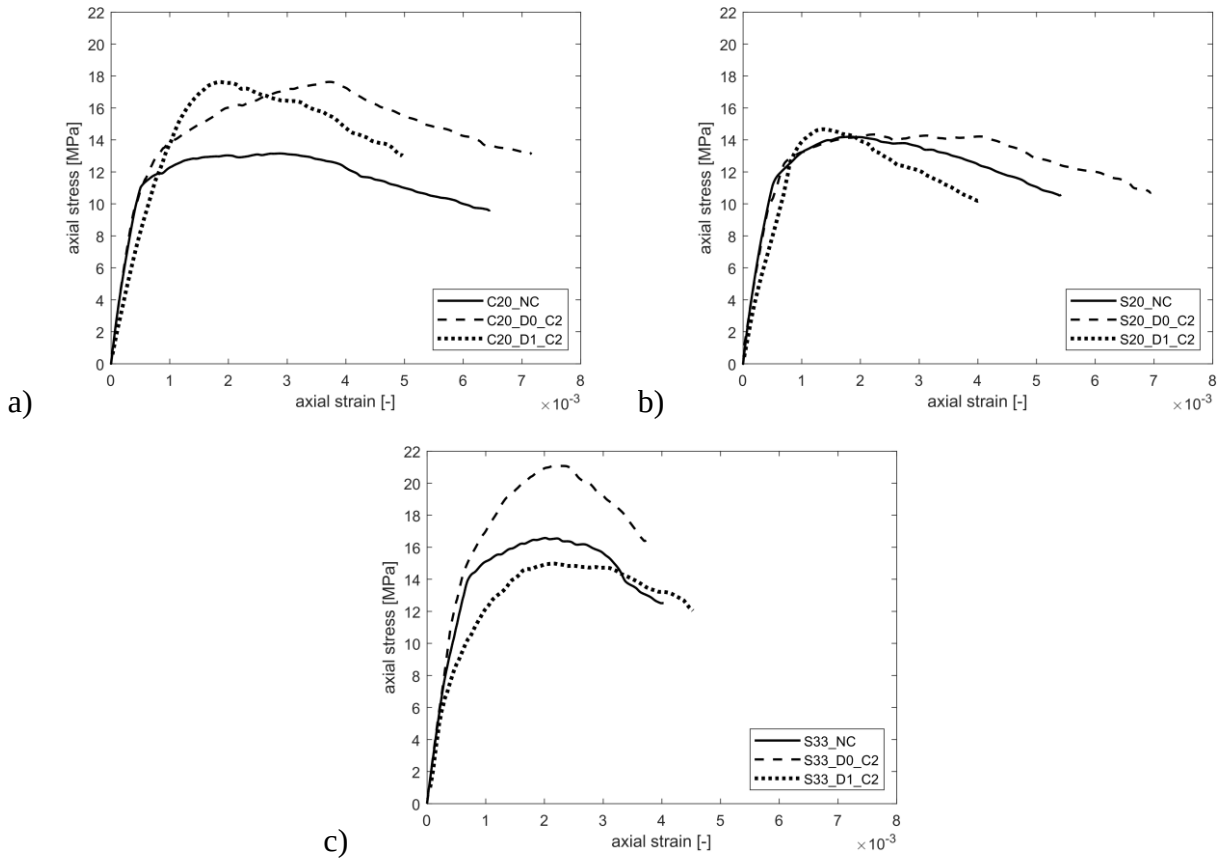

Figure 6. Axial stress strain behavior of the considered unconfined (NC), undamaged strengthened (D0) and damaged repaired (D1) specimens.

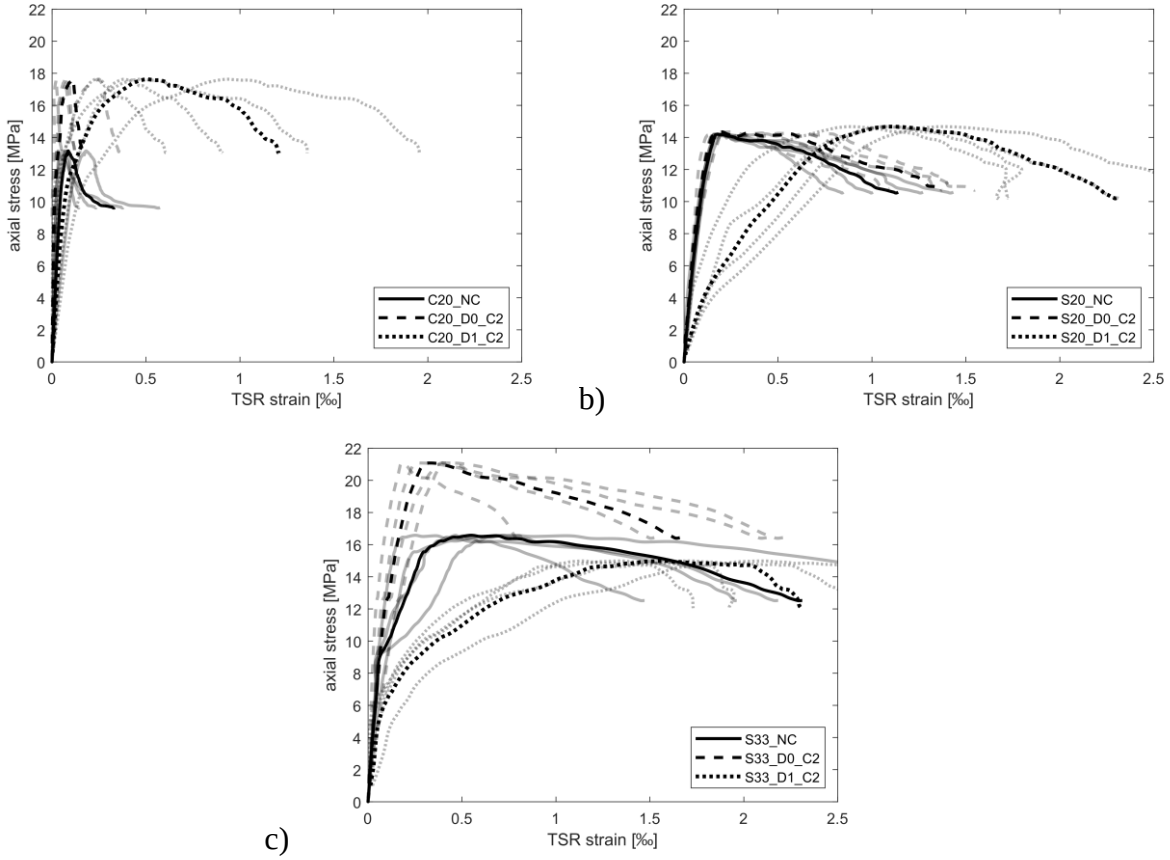

Figure 7. Axial stress – TSR strains for unconfined, undamaged strengthened and damaged repaired columns. (a) C20, b) S20 and c) S_33 specimens

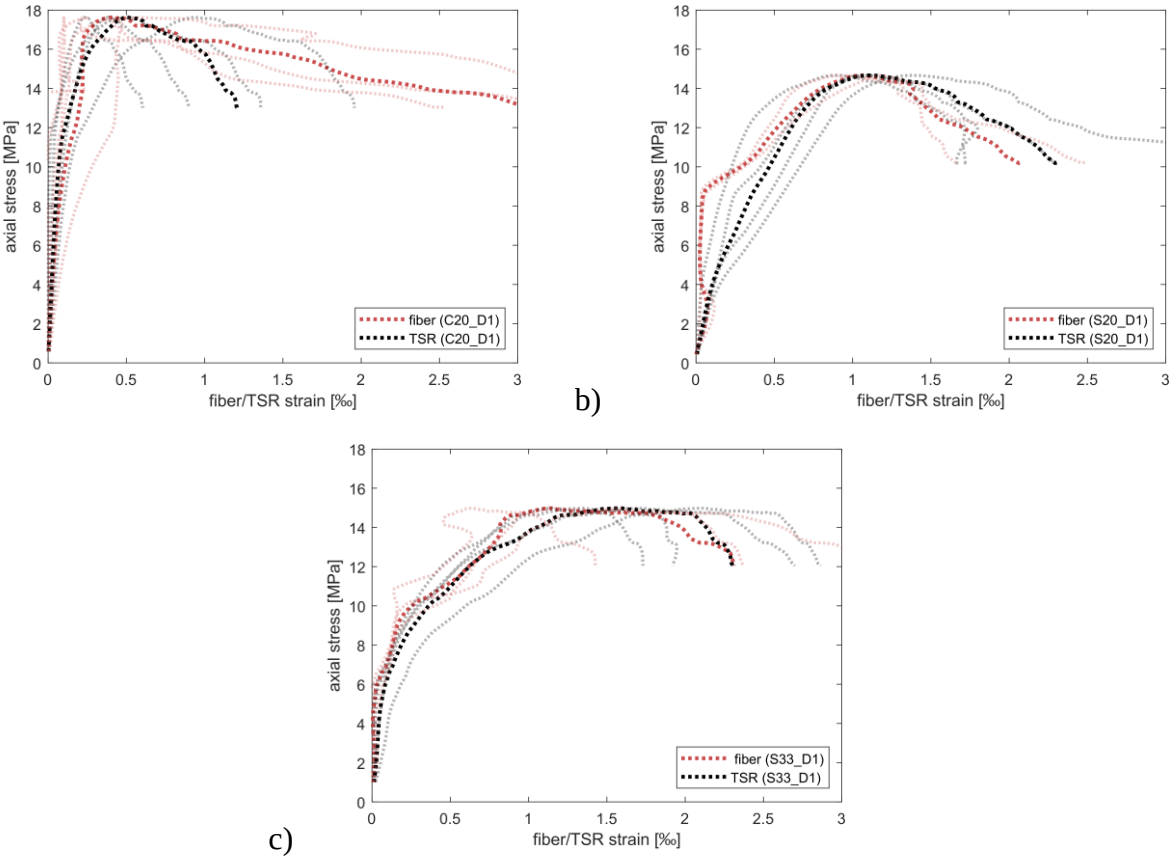

Figure 8. Axial stress – fiber and TSR strain for damaged repaired specimens. a) C20_D1_C2, b) S20_D1_C2, c) S33_D1_C2

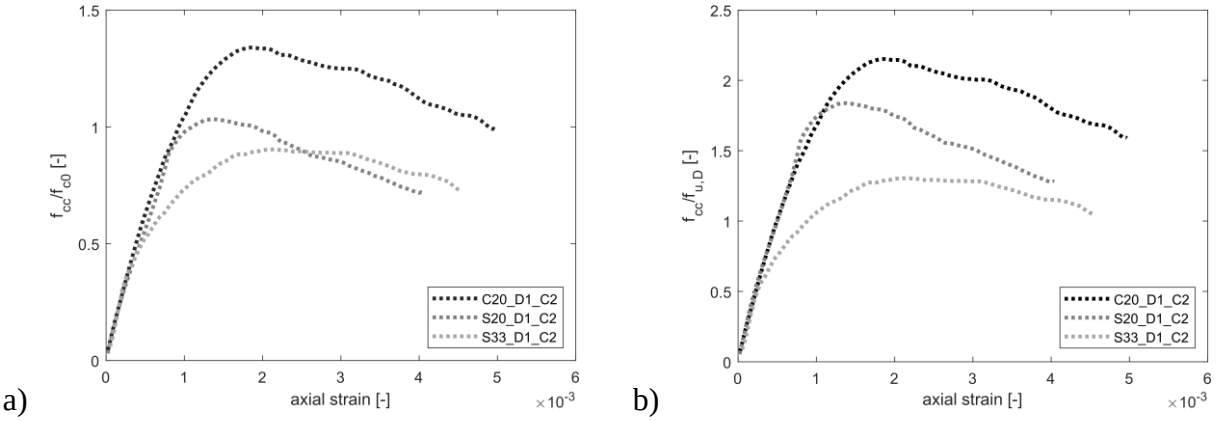

a) b)

Figure 9. Relative axial stress – strain curve with respect to the undamaged cases (a) and to the residual axial capacity of the damaged specimens (b).

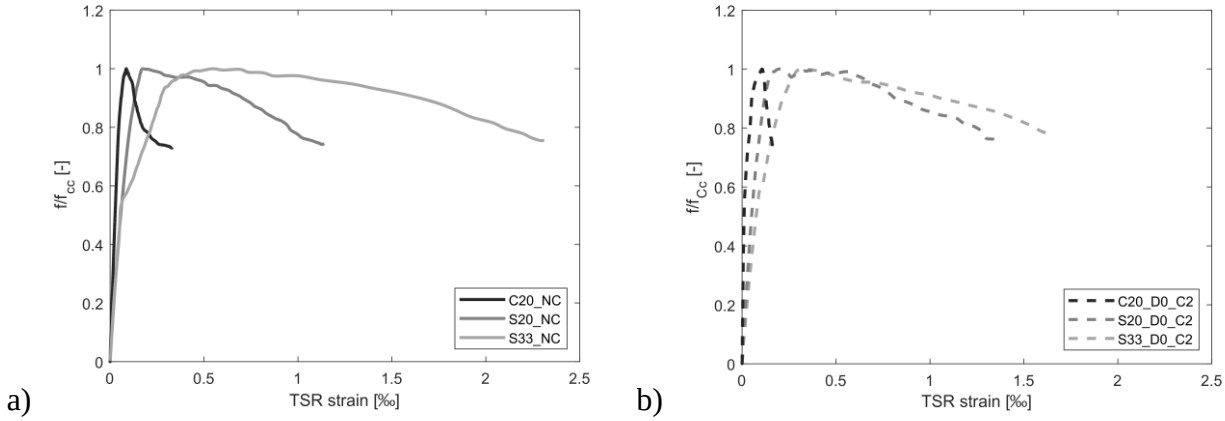

a) b)

Figure 10. TSR strains in unconfined (a) and in undamaged strengthened specimens (b)

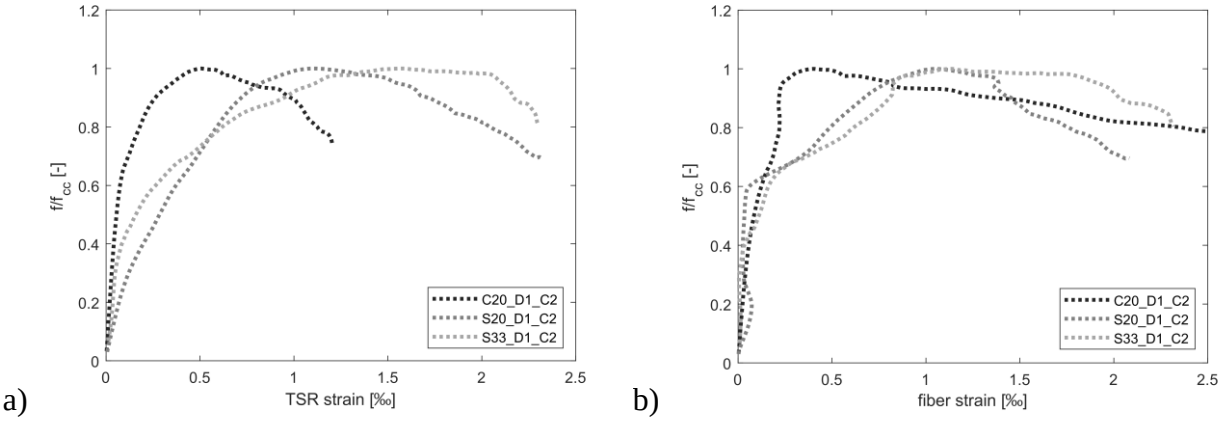

a) b)

Figure 11. TSR (a) and fiber (b) strains in the damaged repaired specimens